Engineered Science
DOI: https://dx.doi.org/10.30919/es919

# A Stable Nonlinear Switched System for Landmark-aided Motion Planning

Sandeep A. Kumar,[1,*] Jito Vanualailai,[1] Bibhya Sharma,[1] Avinesh Prasad[1] and Ravinesh Chand[1, 2]

## Abstract

To guarantee navigation accuracy, the robotic applications utilize landmarks. This paper proposes a novel nonlinear switched system for the fundamental motion planning problem in autonomous mobile robot navigation: the generation of continuous collision-free paths to a goal configuration via numerous land- marks (waypoints) in a cluttered environment. The proposed system leverages the Lyapunov-based control scheme (LbCS) and constructs Lyapunov-like functions for the system's subsystems. These functions guide a planar point-mass object, representing an autonomous robotic agent, towards its goal by utilizing artificial landmarks. Extracting a set of nonlinear, time-invariant, continuous, and stabilizing switched velocity controllers from these Lyapunov-like functions, the system invokes the controllers based on a switching rule, enabling hierarchical landmark navigation in complex environments. Using the well-known stability criteria by Branicky for switched systems based on multiple Lyapunov functions, the stability of the proposed system is provided. A new method to extract action landmarks from multiple landmarks is also introduced. The control laws are then used to control the motion of a nonholonomic car-like vehicle governed by its kinematic equations. Numerical examples with simulations illustrate the effectiveness of the Lyapunov-based control laws. The proposed control laws can automate various processes where the transportation of goods or workers between different sections is required.

*Keywords:* Passive artificial landmarks; Landmark navigation; Switched system; Lyapunov stability; Autonomous systems; Guidance navigation and control; Autonomous mobile robots.
Received: 24 January 2023; Revised: 16 June 2023; Accepted: 18 June 2023.
Article type: Research article.

## 1. Introduction

Integrating robotic systems in aerospace, agriculture, construction, food and beverage, entertainment, health care, pharmaceutical, manufacturing, mining, hospitality, and transportation has benefited humans considerably. These benefits include improved quality of life, safety, increased efficiency, and productivity, and lowered risk of human lives in a hazardous environment. These benefits arise from the successful introduction of different types of robots for transportation, companionship, medical treatment and surgery, search and rescue, pursuit-evasion, packaging, harvesting, assembly, and explorations.[1-3] As a result, several robotic mechanical systems such as unmanned aerial vehicles (UAVs), unmanned ground vehicles (UGVs), unmanned surface vessels (USVs), unmanned underwater vehicles (UUVs), anchored and unanchored robotic arms, mobile manipulators, and assistive and service robots have been the center of research for several decade.[3-7] One of the most common areas of robotic research that has attracted the attention of many researchers is *motion planning*.

Motion planning involves developing a robust algorithm that computes a dynamically feasible trajectory from an initial configuration space to a goal configuration space, ensuring obstacle and collision avoidance while observing system singularities, limitations, and restrictions. Considerable research has been carried out to develop algorithms that solve the findpath problem. Of course, a comprehensive solution to this problem must consider the shortest, smoothest, and safest paths. Over the years, many sophisticated algorithm have been presented by researchers for this findpath problem. These algorithms can be classified into two major categories: classical and heuristic methods. The classical method includes cell decomposition, roadmap, Voronoi graphs, tangent graph, rapidly-exploring random tree (RRT), Dublin's path, probabilistic roadmap, and artificial potential field method.[8] While the Dijkstra algorithm, A$*$ algorithm, artificial neural

[1] *School of Information Technology, Engineering, Mathematics & Physics, The University of the South Pacific, Suva 1168, Fiji.*
[2] *School of Mathematical & Computing Sciences, Fiji National University, Suva 3722, Fiji.*
**Email*: *sandeep.a.kumar@usp.ac.fj* (S. A. Kumar)

networks, genetic algorithms, ant colony optimization, particle swarm optimization, artificial bee colony, differential evolution, Floyd algorithm, fuzzy logic, grey wolf optimization, and bat algorithm belong to the heuristic methods.[9] Artificial Intelligence (AI) algorithms (such as naive bayes, decision tree, random forest, logistic regression, support vector machines, and k nearest neighbours) is a third category that has recently emerged from the heuristic methods, and machine learning is a sub-field of AI.[9]

Moreover, each of the classical and heuristic methods has strengths and weaknesses. Researchers have developed classical hybrid algorithms, heuristic hybrid algorithms, and classical-heuristic algorithms to solve their problems effectively. There is still much focus on developing algorithms that effectively solve the emerging findpath problems. One such problem is motion planning via the concept of landmarks. Landmarks for a planning problem are subgoals,[10] and goals are landmarks as well. Landmarks are mandatory abstract tasks and should be performed by any solution plan. One way to benefit from the landmark concept in solving motion planning problems is by performing hierarchically. Task A must be per- formed before performing task B.[11] For instance, task B is to lay a six-inch block on an eight-inch bock, making laying an eight-inch block task A. Land- marks can also be ordered according to the order they need to be performed. Moreover, if multiple landmarks are present in a workspace, every landmark may not be necessary along a robot's trajectory. The important landmarks extracted from a *landmark verification* process are action landmarks. In the context of robotics, landmarks could be used for robot navigation,[8,12-14] and for self-localization,[15-18]

Landmark-based motion planning is widely researched in robotics and aims to establish a safe motion strategy with optimum trajectories in cluttered environments. As a result, various landmark selection algorithms have been designed and implemented to solve landmark-based navigation problems using different robotic systems. For instance, the semi-definite programming (SDP) algorithm was used on a robotic arm,[19] the Triangulation Based Fusion (TBF) algorithm was applied on a Nomad 200 robot,[20] the Monte Carlo Localization (MCL) algorithm was used to navigate an underwater robot autonomously,[4] and a neuro-fuzzy controller,[9] and LbCS[21] were used for motion control of multiple mobile robots in bounded workspaces via selected landmarks.

However, for the navigation of mobile robots in an obstacle-ridden workspace, selecting the optimal number of landmarks from multiple landmarks is crucial for landmark-based motion planning. Therefore, landmarks selected and provided to the robot in a hierarchy offer a perfect solution for landmark-aided navigation problems. The hierarchal landmark technique was recently implemented on anchored manipulators in Refs. [22] and [23] to acquire precise robotic arm end-effector trajectories. In addition, hierarchal landmarks were also implemented for selecting optimal paths for the car-like mobile robots in Refs. [24] and [25]. Although the concept of hierarchal landmark navigation is recent, it can potentially contribute to significant practical applications such as transportation and loading/offloading items in a constrained environment like docks. This research is inspired by the lack of interest by researchers in incorporating hierarchal landmarks into landmark-based motion planning for autonomous mobile robot navigation.

This paper aims to develop the velocity controllers of a point-mass object, which navigates via hierarchal landmarks to its target in unconstrained and constrained environments. The hierarchal landmarks serve as the waypoints for the point-mass object. Thus, navigating to a distinctive hierarchal landmark will create a separate subsystem. Combining the distinct subsystems will, therefore, create a switched system. A *switched system* is a hybrid dynamical system comprising a family of continuous-time subsystems and includes a law (switching rule) that coordinates the switching between these subsystems.[26] Therefore, the switched velocity controllers will successfully enable the point-mass object to maneuver from its initial position in a *priori* known environment via distinct hierarchal landmarks to its equilibrium state. In terms of detecting and selecting action landmarks amongst the presence of multiple landmarks and obstacles in a cluttered environment, the proposed hierarchal landmark-based navigation is a better approach than those presented in Refs. [24] and [25], which failed to address the vital process of landmark detection and selection. Branicky's work, in 1998, on stable switched and hybrid systems is an interesting theoretical exposition on the intriguing stability properties of such systems that require multiple Lyapunov functions.[27] The stability of the switched system for the arbitrary switching signal in Ref. [27] was established by employing Multiple Lyapunov-like functions. This paper shows that Branicky's criteria can be used to construct a switched system governed by ordinary differential equations (ODEs) for the most basic motion planning problem, the *findpath problem*, in autonomous mobile robot navigation. The stability of the switched system for the arbitrary switching signal is established by employing multiple Lyapunov functions. Using the Lyapunov-based Control Scheme (LbCS), the velocity based-controllers for the point-mass object are derived for each subsystem using the multiple Lyapunov functions. Secondly, a new switching rule will be designed for the switched velocity controllers of the point-mass object, enabling it to extract the action landmarks from several landmarks in its workspace and use those to converge to its goal orientation. Finally, the controllers are applied to a nonholonomic car-like vehicle for landmark navigation. The switched velocity controllers will provide greater mobility and increased access to the robots in a cluttered environment, thereby performing better than the hierarchal landmark-based navigation on anchored manipulators utilized in Refs. [23] and [22]. This novel technique can potentially have real-life applications in the military, health care, logistics, and assembly line production. For instance, in manufacturing,

 

transportation robots could drop off materials at different workstations. The significant contributions of this paper are:
1. design of a new set of nonlinear, time-invariant, continuous, and stabilizing switched velocity controllers for hierarchical landmark navigation in cluttered environments. From the authors' point of view, such stabilizing velocity-based controllers are derived in the sense of Lyapunov for hierarchical landmark-based navigation of mobile robots for the first time. Furthermore, due to LbCS, the controllers' inherent robust nature responds well to system singularities and restrictions. Using the controllers proposed in this research, the mobile robot's mechanical constraints and singularities can be easily captured compared to the landmark-based navigation algorithm utilized in Ref. [20], where the inability to address the system singularities and limitations gave rise to erratic and unstable motion of the mobile robot.
2. a new method for extracting action landmarks, as hierarchal landmarks, from multiple landmarks based on the robot's detection region. The pro- posed approach will perform better in a workspace cluttered with multiple landmarks than the hierarchal landmark-based techniques reported in Refs. [24] and [25], which did not have the feature of selecting and extracting action landmarks. Furthermore, the method presented in this research can be used to automate the process in the industrial sector, especially where items or workers have to be transported or loaded/offloaded from one station to another in a constrained environment.

The remainder of the paper is organized as follows: Section 2 discusses related work. Section 3 gives a brief description of the LbCS. A summary of switched systems and their stability via multiple Lyapunov-like functions is presented in Section 4. Section 5 gives an insight into the find path problem via landmarks. In sections 6 and 7, the velocity control laws are derived, enabling the point-mass object to navigate via hierarchical landmarks in unconstrained and constrained environments. Section 8 presents a switching signal for the point-mass object to extract an action landmark from the landmarks that fall in its detection region. The velocity control laws derived in sections 6, 7, and 8 are applied to the nonholonomic car-like vehicle in Section 9, and simulation studies of the car-like vehicle are presented. Finally, a discussion and concluding remarks are made in sections 10 and 11, respectively.

## 2. Related work

Motion planning is an essential task in the field of robotics. One of the significant challenges for the motion of robotic systems is safe, stable, and reliable autonomous navigation. Many successful robotic applications utilize landmarks along the trajectories to guarantee navigation accuracy. Although many landmarks exist in the natural environment, landmark-based motion planning approaches help select the important landmarks to generate optimal robotic paths.
Landmarks can be generally classified as active and passive. According to Miguel *et al.*,[28] active landmarks actively send location information such as radio waves or satellite signals using radio, ultrasound, and Global System Position (GPS) to the robot, which processes information using receivers to convert the satellite signals into position, velocity, and time estimates to aid in navigation. In 2002, Tedder *et al.*,[29] studied the effectiveness of GPS satellite position data consisting of grid coordinates on a Bearcat robot to navigate to a given sequence of predefined waypoints while avoiding obstacles. The GPS navigation algorithm was utilized as a feedback control loop that guided the robot around the path obstacle and the target point. However, poor accuracy of the GPS was a significant drawback in this research which the authors overcame by installing more ground-based receivers on the robot. Although active landmark systems like the GPS method are widely used in transmitting signals about locations for robot motion, this solution is impractical in indoor applications where satellite signals are not reliable.[28]

On the other hand, passive landmarks do not actively transmit signals; rather, the robot detects location information through sensors. The identification and location of landmarks are directly linked to the number and type of sensors used, as demonstrated by Wang and Yang[9] in 2003, who developed a neuro-fuzzy controller for motion control of a nonholonomic differential drive mobile robot using a combination of four sharp infrared sensors to read the distance to obstacles and landmarks. The controller then processed the distance information to adjust the speed of two separate motors of the robot in passing through the landmarks and obstacle avoidance. In 2009, Vázquez-Martín *et al.*[30] presented a curvature-based environment description for robot navigation using laser range sensors. The laser scan data segmentation algorithms and the segmentation results were used for image processing and to provide position information about the passive landmarks of the robot environment in the form of line and curve segments, corners, and edges.

Passive landmarks can be further categorized as natural and artificial types. Natural landmarks are the distinct features extracted from the entire robot workspace without any changes being made in the structuring of the environment, with most systems utilizing sensory data and motion control schemes for navigation and identification of the natural environment.[30] For example, the extraction and matching of natural point landmarks were studied by Wijk *et al.*[20] in 2000, who utilized the Triangulation Based Fusion (TBF) algorithm for filtering out stable two-dimensional points from raw sonar data to autonomously navigate a Nomad 200 robot from one room to another in a building. However, the navigation results revealed that the robot acquired information on many ghost (mismatched) landmarks while navigating through an empty corridor compared to environments full of natural landmarks like the living room and the office. The erratic and unstable motion could have been avoided by continuously updating the robot on the locations of the nearest land- marks on the reference map. Furthermore, the work of Wijk *et al.* revealed a disadvantage of using natural landmarks which was the

difficulty in making a precise position measurement of distant landmarks, with its usage limited to structured, office-like environments containing a sufficient number of naturally occurring detectable features.[30]

Compared to natural landmarks, the artificial landmarks technique was more widely used for localization and navigation tasks by researchers in structured industrial applications. Bączyk *et al.* claimed in their study that the use of artificial landmarks as visual cues could improve operational characteristics of vision-based methods in contrast to the recognition of natural environment features.[31] Artificial landmarks are features that are set up and unobtrusively added to the environment for easier recognition and detection by the robot's sensors and motion control schemes.[23] Bączyk *et al.*[31] in 2003 presented a vision-based landmark recognition method for mobile robot localization in partially known environments. Simple, unobtrusive artificial landmarks were used as external localization aids that enabled unambiguous global localization in detecting the position and orientation of the robot relative to the landmark. Later in 2014, Kim *et al.*[4] proposed a novel vision-based object detection technique based on artificial landmarks and applied it to the Monte Carlo Localization (MCL) algorithm, a map-based localization technique, with an underwater robot platform in structured underwater environments. A two-step approach, comprising the image processing and localization steps, was utilized to successfully apply the landmark detection results to MCL for navigation in harsh underwater conditions.

Landmark recognition is considered one crucial research area in robot navigation systems. Besides distant landmarks stored redundantly, landmarks close to the robot's trajectory may not necessarily be suitable or important in a robot's trajectory, especially in a workspace with multiple landmarks. This prompted researchers to introduce a hierarchy in the landmark structure and use practical landmarks with accurate position information to navigate robotic systems precisely. In 2020, Prasad *et al.*[24] used the concept of strategic creation and positioning of landmarks in a bounded workspace to guide the robot to navigate the workspace safely and park accurately inside a designated parking bay. The car-like robot maneuvered from one newly fixed landmark to another before finally converging on a target with a pre-defined posture. Landmarks were placed at regular intervals in front of the parking bay to guide the car-like vehicle to its target and park correctly. Kumar *et al.*[25] in 2021 used switched LbCS-based control laws for motion control of a Lagrangian swarm of UGVs via hierarchal landmarks in a cluttered environment. Although the switched system was successfully shown to be stable in the sense of Lyapunov, the system's scalability was not guaranteed, which was a drawback of this approach.

Apart from mobile robots, hierarchal landmarks were also recently implemented on anchored manipulators to acquire precise end-effector trajectories. Anchored robotic arms were proposed and utilized by Chand *et al.* in 2020[22] and 2021[23] to demonstrate that robotic arms in an automated assembly line could navigate via hierarchal landmarks and perform several repetitive tasks which are in hierarchal order. The stabilizing two-dimensional switched controllers were derived in both studies with multiple Lyapunov functions to enable the *n*-link robotic arms to perform multiple tasks in one sequence while observing the system restrictions and limitations. However, unexpected algorithm singularities resulting from local minima issues during navigation were a major drawback of this approach.[23]

In robotic environments consisting of multiple landmarks, searching for techniques that could provide the best and most cost-effective route for the robot to reach its goal autonomously by selecting an optimal number of wayward points still prevails. In 2007, Lerner *et al.*[19] used the semi-definite programming (SDP) algorithm as an integer-programming problem on 6 degrees of freedom (6-DOF) robotic arm to select different task-oriented subsets from the available landmarks automatically. In addition, a linearized objective function was formulated into a landmark selection algorithm by Beinhofer *et al.*[32] in 2013 for selecting a set of landmarks suitable for robust navigation of mobile robots that repeatedly executed the same trajectory. Then, in 2020, Sharma *et al.*[21] used LbCS to navigate multiple car-like robots in a bounded workspace via selected landmarks. The landmarks were used as waypoints or navigation aids for guiding the car-like robots to their targets in a constrained workspace comprising fixed obstacles of numerous sizes.

Various methods for solving landmark-based navigation tasks in applications of robotic systems have been presented in the literature. Furthermore, research on the contributions of different types of landmarks for robot navigation is ongoing, mainly focusing on satellite signals, mapping, localization, sensor- based, and motion control algorithms. Compared to the landmark navigation techniques discussed above, this paper presents a new method for detecting and extracting action landmarks from multiple landmarks using a Lyapunov-based hybrid dynamical switched system for autonomous mobile robot navigation via hierarchal landmarks in unconstrained and constrained environments.

## 3. Lyapunov-based Control Scheme

This research utilizes an artificial potential field technique known as the Lyapunov-based control scheme. The development of attractive and repulsive potential field functions is the primary intention of LbCS. These are developed using the distance functions. The attractive potential function at an arbitrary time is the measure of the Euclidean distance between the target and a robot, usually multiplied with the target convergence parameter. The target conver- gence parameter represents the strength of attraction between the target, and the robot. A larger parameter value indicates that the robot converges faster to its target. Whereas, for instance, the repulsive potential function for stationary obstacle avoidance at an arbitrary time is a measure of the ratio of an obstacle avoidance parameter to the Euclidean distance

 

between the stationary obstacle and the robot. The obstacle avoidance parameter represents the strength of repulsion between the stationary obstacle, and the robot. A larger avoidance parameter value indicates that the robot will experience greater repulsion as it approaches the obstacle. Subsequently, these functions are part of a total potential function called the Lyapunov function from which one could extract the time-invariant nonlinear velocity or acceleration controllers.[6,3] Using LbCS, designing controllers is easy, while the controllers are continuous which are its strengths. It is also easy to include control conditions, specifications, inequalities, and mechanical constraints of mechanical systems in the controllers through mathematical functions. The main disadvantage of LbCS is that algorithm singularities (local minima) can be introduced. The reader is referred to Ref. [33] for a detailed account of the LbCS.

An illustration of the LbCS is given utilizing Fig. 1(a) and Fig. 1(b). Fig. 1(a) shows the contour plot generated over a workspace $-10 < Z_1 < 150$ and $-10 < Z_2 < 150$ for a robot whose initial position is at $(10, 10)$. The dashed line is the robot's trajectory from its initial position to its target position $(100, 100)$ which shows the robot avoids the obstacle positioned at $(50, 50)$. Fig. 1(b) shows the 3D visualization of the attractive and repulsive potential fields. The blue line shows the Lyapunov function, which shows that the energy of the robot is monotonically decreasing and is zero at the target position.

## 4. Continuous Switched Systems and Multiple Lyapunov Functions

A switched system is a hybrid dynamical system made up of a family of continuous-time subsystems and a rule that orchestrates switching between them.[26] A switched system is of the form

$$X'(t) = F_i(X(t)), i \in Q := \{1, \ldots, N\} \quad (1)$$

where $X(t) \in \mathbb{R}^n$.[27] It has the following switching rules: (i) each $F_i$ is globally Lipschitz continuous and (ii) the i's are chosen in such a way that there are finite switches in finite time. It is assumed that $F_i(0) = 0$, which means that the individual subsystems have the origin as the equilibrium point. A continuous switched system has the additional rule that the state of (1) does not jump at the switching instants. This means that if there is a switch from $F_{i_{j-1}}$ to $F_{i_j}$ at times $t_j$, $j = 1, 2, 3, \ldots, N$, then $F_{i_{j-1}}(X(t_{j-1}), t_j) = F_{i_j}(X(t_j), t_j)$.

For (1), Branicky[27] further defines the anchored switching sequence, indexed by an initial state $X_0 := X(t_0)$, $t_0 \geq 0$, as

$$S = X_0: (i_0, t_0), (i_1, t_1), \ldots, (i_M, t_M), \ldots, \quad (2)$$

which may be finite or infinite.[27] It completely describes the trajectory of system (1), denoted by $X_S(t)$, according to the rule $(i_j, t_j)$; that is, the rule states that the system evolves according to $X'(t) = F_{i_j}(X(t), t), t_j \leq t \leq t_{j+1}$.

The switching is assumed to be minimal. This means that $i_j \neq i_{j+1}, j \in \mathbb{Z}_+$, the set of non-negative integers. The end-points at which the ith system is active is denoted S|i.

Further, let $T := t_0, t_1, \ldots, t_M, \ldots$ be a strictly increasing sequence of times. The even sequence of T is $\varepsilon(T): t_0, t_2, \ldots$, and the interval completion $I(T)$ is the set $\cup_{j \in \mathbb{Z}_+} [t_{2j}, t_{2j+1}]$. Thus, $I(S|i)$ is the set of times that the i*th* system is active, up to a set of measure zero.

Finally, V is a candidate Lyapunov function if V is a continuous positive definite function (about the origin 0 where $V(0) = 0$) with continuous partial derivatives.

**Definition 4.1.** Given a strictly increasing sequence of times T in $\mathbb{R}$, then V is Lyapunov-like for function F and trajectory $X(\cdot)$ over T if

- $\dot{V}(X(t)) \leq 0$ for all $t \in I(T)$; and
- V is monotonically nonincreasing on $\varepsilon(T)$.

**Theorem 4.2** (Branicky[27]) Let there be candidate Lyapunov functions $V_i$, $i = 1, \ldots, N$, and vector fields $X'(t) = F_{i_j}(X)$ with $F_i(0) = 0$ for all i. Let S be the set of all switching sequences associated with the system. If for each $S \in \mathbf{S}$ and for all i, $V_i$ is Lyapunov-like for $F_i$ and $X_S(\cdot)$ over S|i, then the system is stable in the sense of Lyapunov.

Note that Branicky used the subscript *N* in (2). However, in general, the number of switches *i* may not equal the number of terms of the sequence *S*; hence *M* has been used. If the

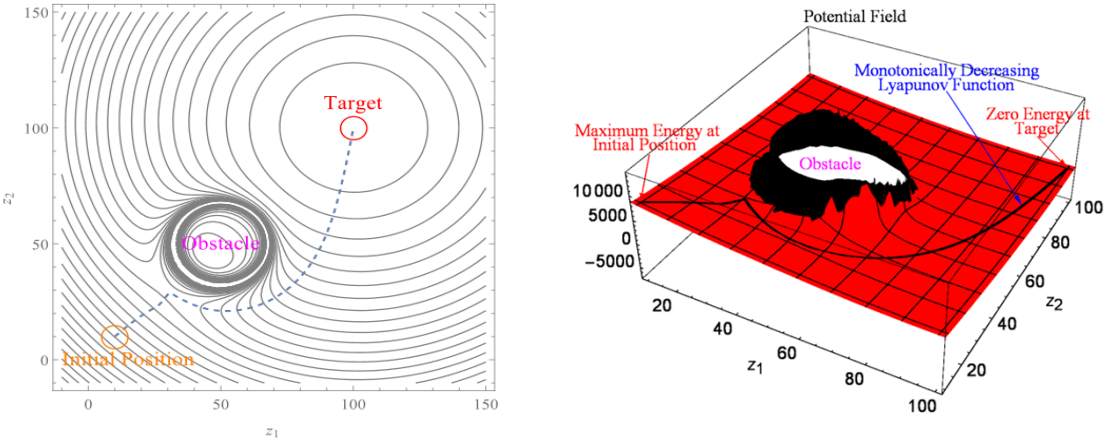


(a) Contour Plot. (b) 3D Visualization

**Fig. 1** An illustration of the Lyapunov-based control scheme.

subsystem $i$ is active only once, then $M = 1$, in which case $S = X_0: (i_0, t_0), (i_1, t_1)$, so that $S|i = \{t_0, t_1\}$ and $I(S|i) = [t_0, t_1]$; however, $\varepsilon(S|i) = t_0$ is not strictly a sequence. In this case, $V_i$ is monotonically nonincreasing on $I(S|i) = [t_0, t_1]$.

## 5. Solving the findpath problem via landmarks

A fundamental problem in robotics is to identify a continuous path that allows a robot, or a part of it, to reach its destination without colliding with obstacles that may exist in the workspace. This is the *findpath problem* [34, 35]. At the most basic level, it involves the construction of mathematical controllers (velocity or acceleration controllers) that allow a point-mass object, representing a robotic agent governed by its kinematic equations, to autonomously navigate to its target in *a priori* known environment. In this paper, a point-mass object in two-dimensional space with position $\big(x(t), y(t)\big)$ at time $t \geq 0$ is considered. With the use of a finite number of known landmarks for navigation (Fig. 2), each landmark conveniently marks the switching from one subsystem to another of a switched system governing the motion of the point-mass object via its instantaneous velocity $(x'(t), y'(t))$.

**Definition 5.1** A point-mass object is a disk with radius $\mathrm{r_a} > 0$ positioned at $\big(\mathrm{x(t), y(t)}\big) \in \mathbb{R}^2$ at time $\mathrm{t} \geq 0$

$$\mathrm{B} \coloneqq (z_1, z_2) \in \mathbb{R}^2 : (z_1 - \mathrm{x})^2 + (z_2 - \mathrm{y})^2 \leq \mathrm{r_a^2} \tag{3}$$

The instantaneous velocity of the point-mass object is $\big(\mathrm{v(t), w(t)}\big) \coloneqq (\mathrm{x'(t), y'(t)})$. The general ODE system governing the motion of B is therefore of the form

$$\dot{\mathrm{x}}(\mathrm{t}) = \mathrm{v}\big(\mathrm{x(t), y(t)}\big), \dot{\mathrm{y}}(\mathrm{t}) = \mathrm{w}\big(\mathrm{x(t), y(t)}\big),$$
$$(\mathrm{x_0, y_0}) = \big(\mathrm{x(0), y(0)}\big) \tag{4}$$

Adopt the vector notation $\mathbf{x}(\mathrm{t}) \coloneqq \big(\mathrm{x(t), y(t)}\big)$, and assume that $(\mathrm{v, w})$ has a state feedback law of the form $\big(\mathrm{v(t), w(t)}\big) \coloneqq \big(-\mu \mathrm{f}\big(\mathbf{x}(\mathrm{t})\big), -\varphi \mathrm{g}\big(\mathbf{x}(\mathrm{t})\big)\big)$, for scalars $\mu, \varphi > 0$ and smooth functions $\mathrm{f}\big(\mathbf{x}(\mathrm{t})\big)$ and $\mathrm{g}\big(\mathbf{x}(\mathrm{t})\big)$ to be constructed appropriately later. Using the vector notation $\mathrm{G}(\mathbf{x}) \coloneqq \big(-\mu \mathrm{f}\big(\mathbf{x}(\mathrm{t})\big), -\varphi \mathrm{g}\big(\mathbf{x}(\mathrm{t})\big)\big) \in \mathbb{R}^2$, the state space representation of the point-mass object system can be written as

$$\dot{\mathbf{x}} = \mathbf{G}(\mathbf{x}), \mathbf{x}_0 \coloneqq \mathbf{x}(\mathrm{t_0}). \tag{5}$$

**Definition 5.2** The target for the point-mass object is a disk with center $(\mathrm{a, b})$ and radius $\mathrm{r_\tau}$. It is described as the set

$$\tau \coloneqq \{(z_1, z_2) \in \mathbb{R}^2 : (z_1 - \mathrm{a})^2 + (z_2 - \mathrm{b})^2 \leq \mathrm{r_\tau^2}. \tag{6}$$

**Definition 5.3.** A landmark $\mathbf{x}_{LM_p}$, $\mathrm{p} = 1, 2, \cdots, \mathrm{n}$, is a disk with center $\big(\mathrm{x_{LM_p}}, \mathrm{y_{LM_p}}\big)$ and radius $\mathrm{r_{LM_p}}$. It is described as the set

$$\mathrm{LM_p} = \Big\{(z_1, z_2) \in \mathbb{R}^2 : \big(z_1 - \mathrm{x_{LM_p}}\big)^2 + \big(z_2 - \mathrm{y_{LM_p}}\big)^2 \leq \mathrm{r_{LM_p}^2}\Big\}. \tag{7}$$

**Remark 5.4** The target, $\tau$, can be considered as an additional landmark, that is, $\mathrm{LM_{n+1}} = \tau$. Denote the distance between the initial position $\big(\mathrm{x(t_0), y(t_0)}\big) = (\mathrm{x_0, y_0})$ of the point-mass object and landmark $\mathrm{LM_p}$ by $\mathrm{d_{LM_p}} = \sqrt{\big(\mathrm{x_0 - x_{LM_p}}\big)^2 + \big(\mathrm{y_0 - y_{LM_p}}\big)^2}$. As depicted in Fig. 2, the positions of the landmarks are assumed such that:

$$\mathrm{d_{LM_1}} < \mathrm{d_{LM_2}} < \mathrm{d_{LM_3}} < \cdots < \mathrm{d_{LM_{n+1}}}. \tag{8}$$

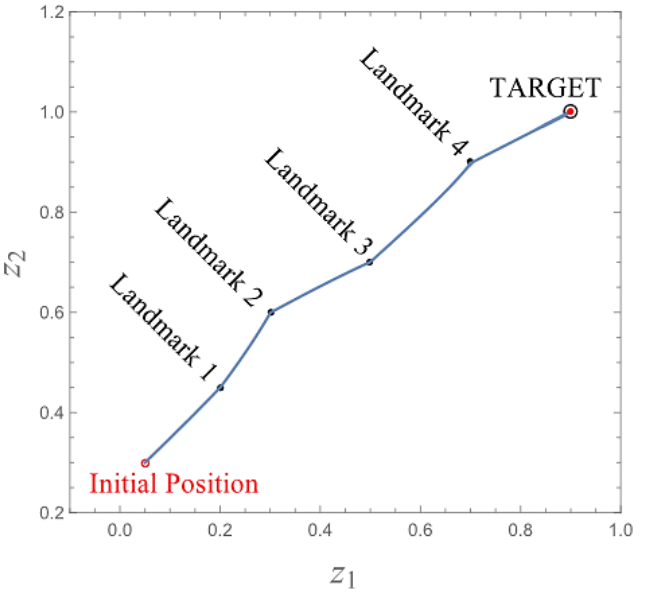


**Fig. 2** Schematic design of the findpath problem for a point-mass object using known landmarks in a workspace.

## 6. Scenario 1: Landmarks in hierarchical order in unconstrained environment

In this case, an environment of the point-mass object free of obstacles is considered. The point-mass object has to start from its initial position, move to its target via landmarks provided in hierarchical order and converge at the target.

### 6.1 Multiple Lyapunov-like functions

In the multiple Lyapunov-like functions to be proposed, the following potential functions will be included:

#### 6.1.1 Landmark attraction function

For the point-mass object to be attracted to the $\mathrm{p^{th}}$ landmark, the following radically unbounded function about a landmark for $\mathrm{p} = \{1, 2, \cdots, \mathrm{n} + 1\}$ is utilized:

$$\mathrm{V_p}(\mathbf{x}) \coloneqq \frac{1}{2}\Big[\big(\mathrm{x - x_{LM_p}}\big)^2 + \big(\mathrm{y - y_{LM_p}}\big)^2\Big]. \tag{9}$$

#### 6.1.2 Auxiliary function

To ensure that the multiple Lyapunov-like functions vanish after the point- mass object has converged to its target $\tau$, the following radically unbounded auxiliary function about the target is utilized:

$$\mathrm{R}(\mathbf{x}) \coloneqq \frac{1}{2}[(\mathrm{x - a})^2 + (\mathrm{y - b})^2]. \tag{10}$$

### 6.2 Multiple Lyapunov-like functions

Introduce $\alpha_\mathrm{p} > 0$ and $\gamma > 0$ as the landmark convergence parameters and target convergence parameter, respectively. Then with respect to each landmark, consider tentative

candidate Lyapunov-like functions of the form,

$$\mathrm{L}_{1_\mathrm{p}}(\mathbf{x}) \coloneqq \gamma \mathrm{R}(\mathbf{x}) + \alpha_\mathrm{p} \mathrm{V}_\mathrm{p}(\mathbf{x}) \mathrm{R}(\mathbf{x}), \quad (11)$$

which are invoked according to the switching rule

$$\mathrm{p} = \begin{cases} 1, & 0 \le \mathrm{d} \le \mathrm{d}_{\mathrm{LM}_1} \\ 2, & \mathrm{d}_{\mathrm{LM}_1} \le \mathrm{d} < \mathrm{d}_{\mathrm{LM}_2} \\ 3, & \mathrm{d}_{\mathrm{LM}_2} \le \mathrm{d} < \mathrm{d}_{\mathrm{LM}_3} \\ \vdots & \\ \mathrm{n}+1, & \mathrm{d}_{\mathrm{LM}_\mathrm{n}} \le \mathrm{d} \le \mathrm{d}_{\mathrm{LM}_{\mathrm{n}+1}}, \end{cases} \quad (12)$$

where $\mathrm{d} = \sqrt{\left(\mathrm{x}(\mathrm{t}) - \mathrm{x}(\mathrm{t}_0)\right)^2 + \left(\mathrm{y}(\mathrm{t}) - \mathrm{y}(\mathrm{t}_0)\right)^2}$.

Along a trajectory of system (5),

$$\begin{aligned} \dot{\mathrm{L}}_{1_\mathrm{p}}(\mathbf{x}) &= \gamma \dot{\mathrm{T}}(\mathbf{x}) + \alpha_\mathrm{p}\left(\dot{\mathrm{V}}_\mathrm{p}(\mathbf{x})\mathrm{T}(\mathbf{x}) + \mathrm{V}_\mathrm{p}(\mathbf{x})\dot{\mathrm{T}}(\mathbf{x})\right) \\ &= \mathrm{f}_{1_\mathrm{p}}(\mathbf{x})\dot{\mathrm{x}} + \mathrm{g}_{1_\mathrm{p}}(\mathbf{x})\dot{\mathrm{y}} \\ &= \mathrm{f}_{1_\mathrm{p}}(\mathbf{x})\mathrm{v} + \mathrm{g}_{1_\mathrm{p}}(\mathbf{x})\mathrm{w}, \end{aligned} \quad (13)$$

where,

$$\mathrm{f}_{1_\mathrm{p}}(\mathbf{x}) = \alpha_\mathrm{p}\mathrm{T}(\mathbf{x})\left(\mathrm{x} - \mathrm{x}_{\mathrm{LM}_\mathrm{p}}\right) + (\mathrm{x} - \mathrm{a})\left(\alpha_\mathrm{p}\mathrm{V}_\mathrm{p}(\mathbf{x}) + \gamma\right) \quad (14)$$

and

$$\mathrm{g}_{1_\mathrm{p}}(\mathbf{x}) = \alpha_\mathrm{p}\mathrm{T}(\mathbf{x})\left(\mathrm{y} - \mathrm{y}_{\mathrm{LM}_\mathrm{p}}\right) + (\mathrm{y} - \mathrm{b})\left(\alpha_\mathrm{p}\mathrm{V}_\mathrm{p}(\mathbf{x}) + \gamma\right) \quad (15)$$

### 6.3 Velocity controllers

Let there be scalars $\mu > 0$ and $\varphi > 0$. Then the velocity controllers are

$$\left.\begin{aligned} v &= -\mu f_{1_p}(\mathbf{x}), \\ w &= -\varphi g_{1_p}(\mathbf{x}) \end{aligned}\right\} \quad (16)$$

where $f_{1_p}(\mathbf{x})$ and $g_{1_p}(\mathbf{x})$ are defined in (14) and (15) respectively.

### 6.4 Stability Analysis

It can be shown that the time derivative of

$$\dot{L}_{1_p}(\mathbf{x}) = -\left[\mu(f_{1_p}(\mathbf{x}))^2 + \varphi(g_{1_p}(\mathbf{x}))^2\right] = -\left[\frac{v^2}{\mu} + \frac{w^2}{\varphi}\right] \le 0. \quad (17)$$

Given (16), system (5) becomes therefore a switched system

$$\dot{\mathbf{x}} = \mathbf{G}_p(\mathbf{x}), \mathbf{x}_0 \coloneqq \mathbf{x}(t_0), p \in \{1,2,\cdots,n+1\}. \quad (18)$$

Since $f_{1_p}(a,b) = g_{1_p}(a,b) = 0$, it is clear that an equilibrium point of system (18) is $\mathbf{x}_e = (a,b)$. Since it is the center of the circular target $\tau$, it is an isolated equilibrium point. Therefore, it can be concluded that:

$$(i) \quad L_{1_p}(\mathbf{x}) > 0 \ \forall \ \mathbf{x} \in \mathbb{R}^2\{\mathbf{x}_e\}, (ii) \quad L_{1_p}(\mathbf{x}_e) = 0, (iii) \quad \dot{L}_{1_p}(\mathbf{x}) \le 0 \ \forall \ \mathbf{x} \in \mathbb{R}^2. \quad (19)$$

Properties (i) and (ii), together with the fact that $L_{1_p}(\mathbf{x})$, $p = \{1,\dots,n+1\}$, have continuous partial derivatives at every point $(x,y) \in \mathbb{R}^2$, it can be concluded that $L_{1_p}(\boldsymbol{x})$ are indeed Lyapunov-like functions for system (18). Now, with $f_{1_p}$ and $g_{1_p}$, it is easy to see that:

$\boldsymbol{G}_p(\mathbf{x}) = \left(-\mu f_{1_p}(\mathbf{x}), -\varphi g_{1_p}(\mathbf{x})\right) \in C^1[\mathbb{R}^2, \mathbb{R}^2]$; indeed, $\boldsymbol{G}_p$ has infinitely many continuous partial derivatives. Thus, $\boldsymbol{G}_p$ is locally Lipschitz continuous. This implies a solution $\boldsymbol{x}(t)$ of system (18) exists and is unique on some time interval $[t_0, s]$, $s > 0$.

**Proof:**

$$\begin{aligned} \| \boldsymbol{G}_p(\mathbf{x}) \| &= \sqrt{\left(-\mu f_{1_p}(\mathbf{x})\right)^2 + \left(-\varphi g_{1_p}(\mathbf{x})\right)^2} \\ &\le \mu|f_{1_p}(\mathbf{x})| + \varphi|g_{1_p}(\mathbf{x}))| \\ &\le (\mu+\varphi)\alpha_p R(\mathbf{x})\left(\left|x - x_{LM_p}\right| + \left|y - y_{LM_p}\right|\right) + \\ &(\mu+\varphi)\left(\alpha_p V_p(\mathbf{x}) + \gamma\right)(|x-a| + |y-b|). \end{aligned}$$

By (8), for all $p = 1,2,\dots,n$, and $(x,y) \in \mathbb{R}^2$, there is $\sqrt{(x - x_{LM_p})^2 + (y - y_{LM_p})^2} < \sqrt{(x-a)^2 + (y-b)^2}$ and $V_p(x) < R(\boldsymbol{x})$. Thus,

$$\begin{aligned} \| \boldsymbol{G}_p(\mathbf{x}) \| &\le (\mu+\varphi)\left[\alpha_p R(\mathbf{x}) + \alpha_p V_p(\mathbf{x}) + \gamma\right](|x-a| \\ &\quad + |y-b|) \\ &\le (\mu+\varphi)\left[2\alpha_p R(\boldsymbol{x}) + \gamma\right](|x-a| + |y-b|) \end{aligned}$$

By (19), $L_{1_p}(\mathbf{x}) = \gamma R(\mathbf{x}) + \alpha_p V_p(\mathbf{x}) R(\mathbf{x}) \le L_{1_p}(\mathbf{x}_0)$ for all $\mathbf{x} \in \mathbb{R}^2$. Thus $R(\mathbf{x}) \le L_{1_p}(\mathbf{x}_0)/\gamma$, and

$$\begin{aligned} \| \boldsymbol{G}_p(\mathbf{x}) \| &\le (\mu+\varphi)\left(2\frac{\alpha_p}{\gamma} L_{1_p}(\mathbf{x}_0) + \gamma\right)(|x-a| \\ &\quad + |y-b|). \end{aligned}$$

Accordingly, for some constant $K > 0$ independent of $s$, there is $\| \boldsymbol{G}_p(\mathbf{x}) \| \le M \| \mathbf{x} - \mathbf{x}_e \|$. Let $\boldsymbol{u} = \mathbf{x} - \mathbf{x}_e$. Then

$$\frac{1}{2}\frac{d}{dt}\| \boldsymbol{u}(t) \|^2 = \langle \boldsymbol{u}(t), \dot{\boldsymbol{u}}(t) \rangle = \left\langle \boldsymbol{u}(t), \boldsymbol{G}_p\left(\mathbf{x}(t)\right) \right\rangle \le \| \boldsymbol{u}(t) \| \| \boldsymbol{G}_p\left(\mathbf{x}(t)\right) \| \le K \| \boldsymbol{u}(t) \|^2. \quad (20)$$

Let $z(t) \coloneqq \| \boldsymbol{u}(t) \|^2$. Then, the differential inequality is

$$\frac{1}{2}\frac{d}{dt} z(t) \le K z(t), z(t_0) = \| \boldsymbol{u}(t_0) \|^2. \quad (21)$$

Comparing (20) and (21), it is easy to see that $\| \boldsymbol{u}(t) \|^2 \le \| \boldsymbol{u}(t_0) \|^2 \, e^{2K(t-t_0)}, t \in [t_0, s]$.

This implies the existence of the solution $\mathbf{x}(t)$ of system (18) on $[t_0, s+\rho]$, $\rho > 0$ being independent of $s > 0$. Hence, it can be concluded that $\boldsymbol{G}_p(\mathbf{x})$ is globally Lipschitz continuous. It is clear that the multiple candidate Lyapunov functions are of the same type. Thus, system (18) has the simple switching sequence $S = (x_0, y_0): (p_0, t_0), (p_1, t_1)$ for $p = \{1, \dots, n+1\}$, to easily obtain the trajectory $(p_0, t_0): \dot{\mathbf{x}} = \boldsymbol{G}_{p_0}(\mathbf{x}(t), t)$ for $t_0 \le t < t_1$. By property (ii) in (19), one can conclude that $L_{1_p}$ is monotononically decreasing on $I(S|p)$. Hence, $L_{1_p}$ are Lyapunov-like functions satisfying Theorem 4.2. Accordingly, system (18) is stable in the sense of Lyapunov.

**Example 6.1** In this example, $n = 3$ landmarks are considered besides the target, i.e., $p = 1,2,3,4$. System (18), with parameters $\mu = \varphi = 1$, $\alpha_p = 0.05$ and $\gamma = 0.00003$, was numerically integrated via the RK4 method with $t \in [0,5000]$ and step-size 0.1. The end-points of the times that system $p$ was active and the interval completions are

$$\begin{aligned} S|1 &= \{0.0, 416.5\}, & I(S|1) &= \{[0.0, 416.5]\}, \\ S|2 &= \{416.6, 1091.0\}, & I(S|2) &= \{[416.6, 1091.0]\}, \\ S|3 &= \{1091.1, 2839.4\}, & I(S|3) &= \{[1091.1, 2839.4]\}, \\ S|4 &= \{2839.5, 5000.0\}, & I(S|4) &= \{[2839.5, 5000.0]\}. \end{aligned}$$

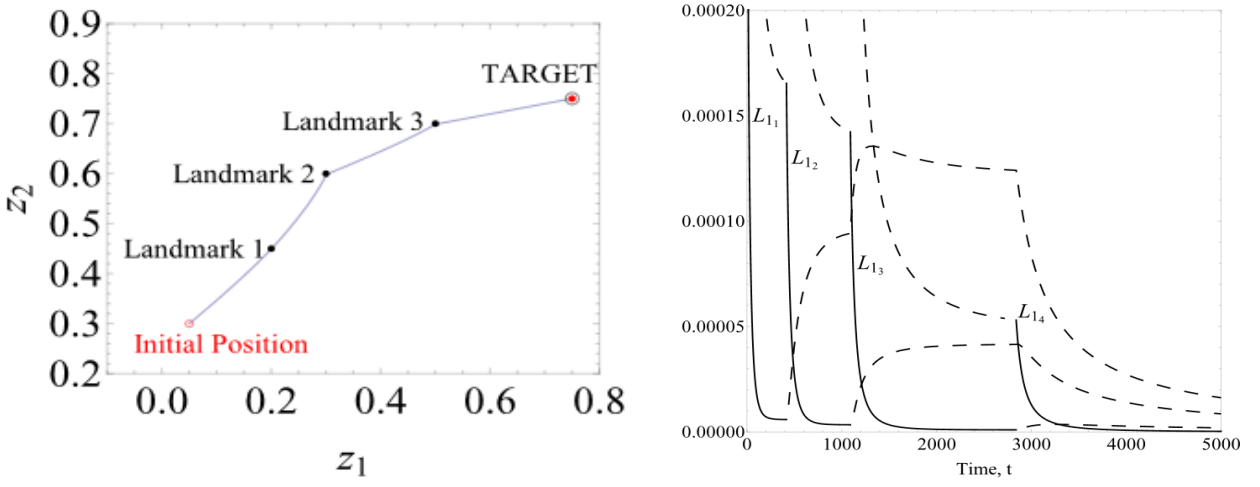


(a) Trajectory of system (18) (b) Multiple Lyapunov functions

**Fig. 3** (a) Trajectory of the point-mass object from its initial position to its target via landmarks. (b) $L_{1_p}(\mathbf{x})$ decreases on each interval where the p[th] subsystem is active.

The trajectory, shown in Fig. 3(a), obeys the rule

$(1_0, 0.0)$: $\dot{\mathbf{x}} = \boldsymbol{G}_{1_0}(\mathbf{x}(t), t), 0.0 \leq t < 416.5,$

$(2_0, 416.6)$: $\dot{\mathbf{x}} = \boldsymbol{G}_{2_0}(\mathbf{x}(t), t), 416.6 \leq t < 1091.0,$

$(3_0, 1091.1)$: $\dot{\mathbf{x}} = \boldsymbol{G}_{3_0}(\mathbf{x}(t), t), 1091.1 \leq t < 2835.4,$

$(4_0, 2839.5)$: $\dot{\mathbf{x}} = \boldsymbol{G}_{4_0}(\mathbf{x}(t), t), 2839.5 \leq t < 5000.0.$

The monotonically decreasing Lyapunov functions are shown in Fig. 3(b).

## 7. Scenario 2: Landmarks in Hierarchical order in Constrained Environments

Now, consider the configuration space of switched system (5) clustered with $q \in \mathbb{N}$ stationary obstacles and $n \in \mathbb{N}$ landmarks.

The $k^{th}$ solid stationary obstacle is a disk with center $(o_{k1}, o_{k2})$ and radius $r_{O_k} > 0$. It is described as the set

$$O_k \coloneqq \{(z_1, z_2) \in \mathbb{R}^2 : (z_1 - o_{k1})^2 + (z_2 - o_{k2})^2 \leq r_{O_k}^2\}. \quad (22)$$

### 7.1 Multiple Lyapunov-like functions

In the multiple Lyapunov-like functions to be proposed, we will utilize landmark attraction function (9) with the following potential functions.

#### 7.1.1 Target attraction function

For target convergence the auxiliary function (10) are modified to

$$H(\mathbf{x}) \coloneqq \frac{1}{2}[(x-a)^2 + (y-b)^2] + \epsilon^2, \quad (23)$$

where $\epsilon > 0$ is a sufficiently small constant. The role of this constant is to ensure that the proposed system satisfies the first switching rule of a switched system.

#### 7.1.2 Stationary obstacle avoidance function

For the purpose of avoiding possible collision with the $k^{th}$ stationary solid obstacle (22) where $k \in 1,2,3,\cdots,q$, the following obstacle avoidance function is utilized:

$$W_k(\mathbf{x}) = \frac{1}{2}\left[(x-o_{k1})^2 + (y-o_{k2})^2 - \left(r_{O_k} + r_a\right)^2\right]. \quad (24)$$

Now, introduce $\beta_k > 0$ as obstacle collision avoidance parameter. Then with respect to each landmark, consider a Lyapunov-like function of the form

$$L_{2_p}(\mathbf{x}) \coloneqq \gamma H(\mathbf{x}) + \alpha_p V_p(\mathbf{x}) H(\mathbf{x}) + \sum_{k=1}^{q} \beta_k \frac{H(\mathbf{x})}{W_k(\mathbf{x})}, \quad (25)$$

which are invoked according to the switching rule

$$p = \begin{cases} 1, & 0 \leq d < d_{LM_1} \\ 2, & d_{LM_1} \leq d < d_{LM_2} \\ 3, & d_{LM_2} \leq d < d_{LM_3} \\ \vdots & \\ n+1, & d_{LM_n} \leq d \leq d_{LM_{n+1}}, \end{cases} \quad (26)$$

where $d = \sqrt{(x(t) - x(t_0))^2 + (y(t) - y(t_0))^2}$.

### 7. 2 Velocity controllers

Let there be scalars $\mu > 0$ and $\varphi > 0$. Then the velocity controllers are

$$\left.\begin{aligned} v &= -\mu f_{2_p}(\mathbf{x}), \\ w &= -\varphi g_{2_p}(\mathbf{x}) \end{aligned}\right\} \quad (27)$$

where

$$f_{2_p}(\mathbf{x}) = \alpha_p H(\mathbf{x})\left(x - x_{LM_p}\right) + \left(\alpha_p V_p(\mathbf{x}) + \gamma + \sum_{k=1}^{q} \frac{\beta_k}{W_k(\mathbf{x})}\right)(x-a) - \sum_{k=1}^{q} \beta_k \frac{H(\mathbf{x})}{W_k^2(\mathbf{x})}(x - o_{k1}) \quad (28)$$

and

$$g_{2_p}(\mathbf{x}) = \alpha_p H(\mathbf{x})\left(y - y_{LM_p}\right) + \left(\alpha_p V_p(\mathbf{x}) + \gamma + \sum_{k=1}^{q} \frac{\beta_k}{W_k(\mathbf{x})}\right)(y-b) - \sum_{k=1}^{q} \beta_k \frac{H(\mathbf{x})}{W_k^2(\mathbf{x})}(y - o_{k2}). \quad (29)$$

### 7.3 Stability analysis

$L_{2_p}(\mathbf{x})$, for $p = 1,2,\cdots,n+1$, is positive over the domain

$$D\left(L_{2_p}(\mathbf{x})\right) \coloneqq \mathbf{x} \in \mathbb{R}^2 : W_k(\mathbf{x}) > 0 \; \forall \; k = 1,2,\ldots,q.$$

Then

$$\dot{L}_{2_p}(\mathbf{x}) = -\left[\mu(f_{2_p}(\mathbf{x}))^2 + \varphi(g_{2_p}(\mathbf{x}))^2\right] = -\left[\frac{v^2}{\mu} + \frac{w^2}{\varphi}\right] \leq 0, \tag{30}$$

for all $\mathbf{x} \in D\left(L_{2_p}(\mathbf{x})\right)$. Given (27), system (5) becomes therefore a switched system

$$\dot{\mathbf{x}} = \boldsymbol{G}_p(\mathbf{x}), \mathbf{x}_0 \coloneqq \mathbf{x}(t_0), p \in 1,2,\cdots,n+1. \tag{31}$$

Looking at the right-hand side of equations (28) and (29), the functions that appear in the denominator are $W_k$, $k \in \mathbb{N}$. Hence, it can be easily concluded that $\boldsymbol{G}_p(\mathbf{x}) = \left(-\mu f_{2_p}(\mathbf{x}), -\varphi g_{2_p}(\boldsymbol{x})\right) \in C^1\left[D\left(L_{2_p}(\mathbf{x})\right), \mathbb{R}^2\right]$ for all $p = 1,2,\cdots,n+1$, which implies that at least on some time interval $[t_0, s]$, $s > 0$, the solution of $\mathbf{x}(t)$ of system (31) exists and is in $D\left(L_{2_p}(\mathbf{x})\right)$. Certainly, since the functions $W_k$ appear in the denominator in (28) and (29), they will also appear in the denominator of higher-order partial derivatives, with each derivative continuous on $D\left(L_{2_p}(\mathbf{x})\right)$. This indicates that $\boldsymbol{G}_p(\mathbf{x})$ is locally Lipschitz on $D\left(L_{2_p}(\mathbf{x})\right)$; that is, $\boldsymbol{G}_p(\mathbf{x}) = \left(-\mu f_{2_p}(\mathbf{x}), -\varphi g_{2_p}(\mathbf{x})\right) \in C^\infty\left[D\left(L_{2_p}(\mathbf{x})\right), \mathbb{R}^2\right]$. This means that the solution of $\mathbf{x}(t)$ exists and is unique on the time interval $[t_0, s]$.

**Proof:**

$$\begin{aligned}
\| \boldsymbol{G}_p(\mathbf{x}) \| &= \sqrt{\left(-\mu f_{2_p}(\mathbf{x})\right)^2 + \left(-\varphi g_{2_p}(\mathbf{x}))\right)^2} \\
&\leq \mu|f_{2_p}(\mathbf{x})| + \varphi|g_{2_p}(\mathbf{x}))| \\
&\leq (\mu+\varphi)\alpha_p H(\mathbf{x})\left(\left|x - x_{LM_p}\right| + \left|y - y_{LM_p}\right|\right) \\
&\quad + (\mu+\varphi)\left(\alpha_p V_p(\mathbf{x}) + \gamma \right. \\
&\quad \left. + \sum_{k=1}^{q} \frac{\beta_k}{W_k(\mathbf{x})}\right)(|x-a| + |y-b|) \\
&\quad + (\mu+\varphi)\sum_{k=1}^{q} \beta_k \frac{H(\mathbf{x})}{W_k^2(\mathbf{x})}(|x - o_{k1}| \\
&\quad + |y - o_{k2}|).
\end{aligned}$$

By (8), for all $p = \{1,2,\ldots,n\}$, and $(x,y) \in \mathbb{R}^2$, there is $\sqrt{(x - x_{LM_p})^2 + (y - y_{LM_p})^2} < \sqrt{(x-a)^2 + (y-b)^2}$ and $V_p(x) < H(\mathbf{x})$. Thus,

$$\begin{aligned}
\| \boldsymbol{G}_p(\mathbf{x}) \| &\leq (\mu+\varphi)\left(\alpha_p H(\mathbf{x}) + \alpha_p V_p(\mathbf{x}) + \gamma \right. \\
&\quad \left. + \sum_{k=1}^{q} \frac{\beta_k}{W_k(\mathbf{x})}\right)(|x-a| + |y-b|) \\
&\quad + (\mu+\varphi)\sum_{k=1}^{q} \beta_k \frac{H(\mathbf{x})}{W_k^2(\mathbf{x})}(|x - o_{k1}| \\
&\quad + |y - o_{k2}|) \\
&\leq (\mu+\varphi)\left(2\alpha_p H(\mathbf{x}) + \gamma + \sum_{k=1}^{q} \frac{\beta_k}{W_k(\mathbf{x})}\right)(|x-a| \\
&\quad + |y-b|) \\
&\quad + (\mu+\varphi)\sum_{k=1}^{q} \beta_k \frac{H(\mathbf{x})}{W_k^2(\mathbf{x})}(|x - o_{k1}| \\
&\quad + |y - o_{k2}|)
\end{aligned}$$

Observe that the time-derivative of $L_{2_p}(\mathbf{x})$ along the solution of (31) is non-positive, which implies that

$$L_{2_p}(\mathbf{x}(t)) \leq L_{2_p}(\mathbf{x}_0) \coloneqq \eta_0, t \in [t_0, s] \tag{32}$$

for all $\mathbf{x} \in D\left(L_{2_p}(\mathbf{x})\right)$. Thus $H(\mathbf{x}) \leq \eta_0/\gamma$, and

$$\begin{aligned}
\| \boldsymbol{G}_p(\mathbf{x}) \| &\leq (\mu+\varphi)\left(2\frac{\alpha_p \eta_0}{\gamma} + \gamma + \sum_{k=1}^{q} \frac{\beta_k}{W_k(\mathbf{x})}\right)(|x-a| \\
&\quad + |y-b|) \\
&\quad + (\mu+\varphi)\sum_{k=1}^{q} \beta_k \frac{H(\mathbf{x})}{W_k^2(\mathbf{x})}(|x - o_{k1}| \\
&\quad + |y - o_{k2}|)
\end{aligned}$$

Similarly, from the form of $L_{2_p}(\mathbf{x})$ in (25), equation (32) implies that for every $k \in \{1,2,\cdots,q\}$,

$$\beta_k \frac{H(\mathbf{x}(t))}{W_k(\mathbf{x}(t))} \leq \eta_0, t \in [t_0, s]. \tag{33}$$

Let $\zeta \coloneqq \min\{\beta_k, \{k \in 1,2,\cdots,q\}\}$. Then, from (33), the following can be obtained:

$$\frac{H(\mathbf{x}(t))}{W_k(\mathbf{x}(t))} \leq \frac{\eta_0}{\zeta} \coloneqq \xi_0, t \in [t_0, s]. \tag{34}$$

Given the form of $H(\boldsymbol{x}(t))$ in (23), the inequality in (34) gives

$$\epsilon^2 \frac{1}{W_k} \leq \frac{H(\mathbf{x}(t))}{W_k(\mathbf{x}(t))} \leq \xi_0, t \in [t_0, s], \tag{35}$$

and hence,

$$\frac{1}{W_k} \leq \epsilon^{-2}\frac{H(\mathbf{x}(t))}{W_k(\mathbf{x}(t))} \leq \epsilon^{-2}\xi_0 \coloneqq \varrho_0, t \in [t_0, s]. \tag{36}$$

Let $\beta_0 \coloneqq \max\{\beta_k, \{k \in 1,2,\cdots,q\}\}$. Then, the following function is obtained using the inequalities (33), (34), (35) and (36):

$$\begin{aligned}
\| \boldsymbol{G}_p(\mathbf{x}) \| &\leq c_1(|x-a| + |y-b|) \\
&\quad + c_2(|x - o_{k1}| + |y - o_{k2}|)
\end{aligned}$$

where the constants $c_1 > 0$ and $c_2 > 0$ independent of $s$. Since the point-mass robot will avoid the obstacles that will fall on its path on its way to its target via the landmarks, therefore

$\| \boldsymbol{G}_p(\mathbf{x}) \| \leq (c_1 + c_2)(|x-a| + |y-b|)$.

Let $c_1 + c_2 = K$, then $\| \boldsymbol{G}_p(\mathbf{x}) \| \leq K \| \mathbf{x} - \mathbf{x}_e \|$. By letting $\boldsymbol{u} = \mathbf{x} - \mathbf{x}_e$, the following can be obtained:

$$\frac{1}{2}\frac{d}{dt}\| \boldsymbol{u}(t) \|^2 = \langle \boldsymbol{u}(t), \dot{\boldsymbol{u}}(t)\rangle = \left\langle \boldsymbol{u}(t), \boldsymbol{G}_p(\mathbf{x}(t))\right\rangle \leq \| \boldsymbol{u}(t) \| \| \boldsymbol{G}_p(\mathbf{x}(t)) \| \leq K \| \boldsymbol{u}(t) \|^2. \tag{37}$$

Let $z(t) \coloneqq \| \boldsymbol{u}(t) \|^2$. Then, the following differential inequality is obtained:

$$\frac{1}{2}\frac{d}{dt}z(t) \le Kz(t), z(t_0) = \| \boldsymbol{u}(t_0) \|^2. \quad (38)$$

Comparing (37) and (38), it is easy to see that $\| \boldsymbol{u}(t) \|^2 \le \| \boldsymbol{u}(t_0) \|^2 \, e^{2K(t-t_0)}, t \in [t_0, s]$.

This implies the existence of the solution $\mathbf{x}(t)$ of system (31) on $[t_0, s+\rho]$, $\rho > 0$ being independent of $s > 0$. Hence, it can be concluded that $\boldsymbol{G}_p(\mathbf{x})$ is globally Lipschitz continuous on $D\left(L_{2_p}(\mathbf{x})\right)$.

It is clear that the multiple candidate Lyapunov-like functions of the same type $L_{2_p}(\mathbf{x})$. Thus, system (31) has the simple switching sequence $S = (x_0, y_0): (p_0, t_0), (p_1, t_1)$ for $p = \{1, \dots, n+1\}$, to easily get the trajectory $(p_0, t_0): \dot{\mathbf{x}} = \boldsymbol{G}_{p_0}(\mathbf{x}(t), t)$ for $t_0 \le t < t_1$. One can conclude that $L_{2_p}(\mathbf{x})$ is monotononically nonincreasing on $I(S|p)$. Hence, $L_{2_p}(\mathbf{x})$ are Lyapunov-like functions satisfying Theorem 4.2. Accordingly, system (31) is stable in the sense of Lyapunov.

**Example 7.2** In this example, $n = 3$ landmarks are considered besides the target, i.e., $p = 1,2,3,4$ with 6 randomly generated obstacles. System (31), with parameters $\mu = \varphi = 1$, $\alpha_p = 0.6$, $\gamma = 0.0008$ and $\beta_k = 0.00000001$, was numerically integrated via the RK4 method with $t \in [0,350]$ and step-size 0.1. The end-points of the times that system $p$ was active and the interval completions are

$S|1 = \{0.0, 28.9\}$, $I(S|1) = \{[0.0, 28.9]\}$,
$S|2 = \{29.0, 74.0\}$, $I(S|2) = \{[29.0, 74.0]\}$,
$S|3 = \{74.1, 186.5\}$, $I(S|3) = \{[74.1, 186.5]\}$,
$S|4 = \{186.6, 350.0\}$, $I(S|4) = \{[186.6, 350.0]\}$.

The trajectory, shown in Fig. 4(a), obeys the rule

$(1_0, 0.0)$: $\dot{\mathbf{x}} = \boldsymbol{G}_{1_0}(\mathbf{x}(t), t), 0.0 \le t < 28.9$,
$(2_0, 29)$: $\dot{\mathbf{x}} = \boldsymbol{G}_{2_0}(\mathbf{x}(t), t), 29.0 \le t < 74.0$,
$(3_0, 74.1)$: $\dot{\mathbf{x}} = \boldsymbol{G}_{3_0}(\mathbf{x}(t), t), 74.1 \le t < 186.5$,
$(4_0, 186.6)$: $\dot{\mathbf{x}} = \boldsymbol{G}_{4_0}(\mathbf{x}(t), t), 186.6 \le t < 350.0$.

The monotonically decreasing Lyapunov functions are shown in Fig. 4(b).

## 8. Extraction of action landmarks

In this section, the configuration space of a point-mass object to be clustered with q ∈ N stationary obstacles and n ∈ N randomly scattered landmarks are considered. The point-mass object has to autonomously navigate to its target by extracting an action landmark from the landmarks which fall in its detection region.

### 8.1 Detection region

The detection region of the point-mass object is shown in Fig. 5.

**Definition 8.1.** The p[th] landmark is in the detection region of the point-mass object if the following are satisfied:

1. $|\Psi_p - \Phi| \le \psi$,
2. $\left\|\mathbf{x} - \mathbf{x}_{LM_p}\right\| \le r$ and
3. $\left\|\mathbf{x}_{target} - \mathbf{x}_{LM_p}\right\| \le \left\|\mathbf{x} - \mathbf{x}_{target}\right\|$

where

• $\Psi_p$ is the angle between $\mathbf{x}$ (the point-mass object) and $\mathbf{x}_{LM_p}$ (the $p^{th}$ landmark) measured counterclockwise.
• $\Phi$ is the angle between $\mathbf{x}$ and $\mathbf{x}_{target}$ (target).
• $\psi$ is the half of the sector angle for the detection region. The detection region is $\psi$ degrees clockwise and counterclockwise from the imaginary line joining the points $\mathbf{x}$ and $\mathbf{x}_{target}$.
• $r$ is the detection range.
• $\left\|\mathbf{x} - \mathbf{x}_{LM_p}\right\|$ is the distance between the point-mass object and the $p^{th}$ landmark.
• $\left\|\mathbf{x}_{target} - \mathbf{x}_{LM_p}\right\|$ is the distance between the target point and the $p^{th}$ landmark.
• $\left\|\mathbf{x} - \mathbf{x}_{target}\right\|$ is the distance between the point-mass object and the target.

Since the target of the point-mass object is also treated as a landmark, there are $n+1$ landmarks scattered in the configuration space of the point-mass object. Let the set $M = \bigcup_{p=1}^{n+1} S_p$ contain all the landmarks that are in the detection region of the point-mass object where,

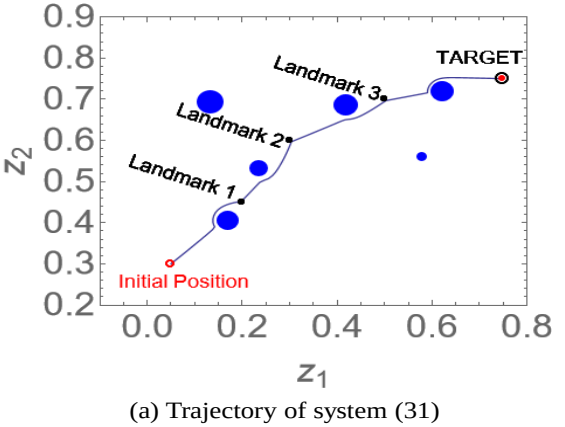


(a) Trajectory of system (31)

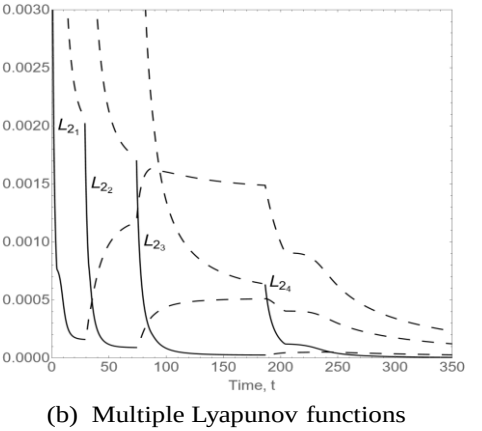


(b) Multiple Lyapunov functions

**Fig. 4** (a) Trajectory of the point-mass object from its initial position to its target via landmarks. (b) $L_{2_p}(\mathbf{x})$ decreases on each interval where the p[th] subsystem is active.

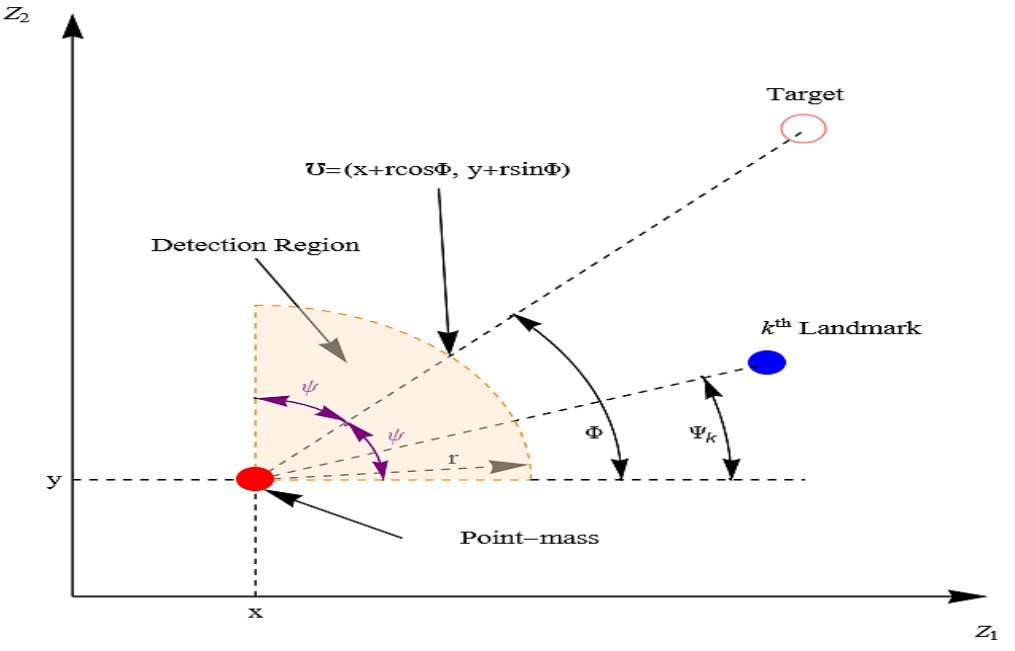


**Fig. 5** Detection region of a point-mass object.

$$S_p = \begin{cases} \{p\}, & if\ |\Psi_p - \Phi| \le \psi\ and\ \left\|\mathbf{x} - \mathbf{x}_{LM_p}\right\| \le r\ and\ \left\|\mathbf{x}_{target} - \mathbf{x}_{LM_p}\right\| \le \left\|\mathbf{x} - \mathbf{x}_{target}\right\| \\ \{\}, & otherwise. \end{cases}$$

Let $M_k$ be the $k$th element of $M$ and let $|M| \le n+1$ be the cardinality of $M$. The Lyapunov-like functions $L_{2_p}(\mathbf{x})$ in (25) will now be invoked according to the switching rule

$$\alpha_p = \begin{cases} \lambda, & if\ p \in M\ and\ D_p = \min\{d_1, d_2, \dots, d_{|M|}\} \\ 0, & otherwise \end{cases} \quad (39)$$

where $\lambda > 0$ and $d_p = \left\|\upsilon - \mathbf{x}_{LM_p}\right\|$. This switching rule with the control laws (27) will ensure that the point-mass object minimizes the cost, which is the Euclidean distance. It simply means that it does not allow the point-mass object to deviate significantly from the shortest path to the target. That is, it extracts the landmark which is closest to the target from the detection region. While the point-mass object is making its way to an action landmark invoked according to the above switching rule, and suddenly if there appears another landmark which now is in the detection region, and is an action landmark, then the point-mass object will start making its way to this new action landmark without reaching the earlier landmark. Thus, the point-mass object does not have to reach a landmark and then move to the other. For instance, a ship does not have to reach a lighthouse which is a landmark for it. The lighthouse is just used as a guide to reaching the target.

**Example 8.2** In this example, the position of the point-mass object with its detection region at different time $t$ during its motion has been shown and captured by Fig. 6. The initial and final positions of the point-mass object are (3,2 and (25,25), respectively. The positions of the $n = 40$ landmarks and $q = 15$ obstacles are randomly generated with $r = 5$ and $\psi = \frac{\pi}{4}$ as the range of the detection region. System (31) and switching rule (39), with parameters $\mu = \varphi = 1$, $\lambda = 0.1$, $\gamma = 0.05$ and $\beta_k = 0.005$, were numerically integrated via the RK4 method.

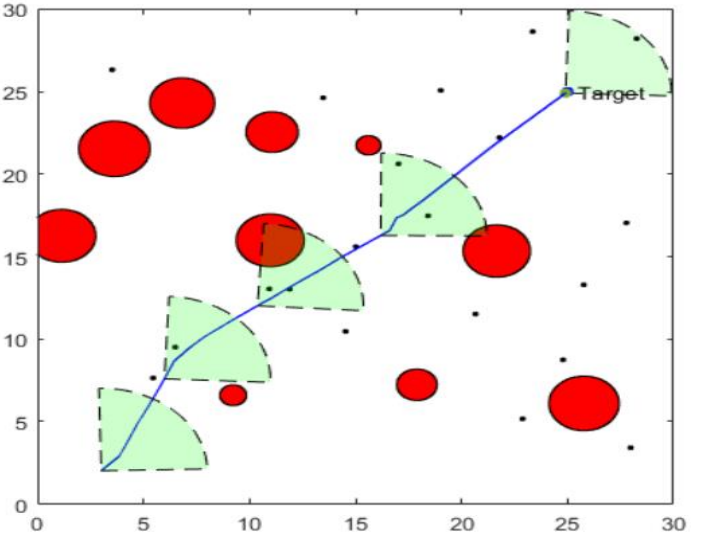


**Fig. 6** Trajectory of the point-mass object from its initial position to its target via extracting landmarks.

## 9. Application to Nonholonomic Vehicle

The nonholonomic vehicle, which is a car-like vehicle mentioned in Ref. [35], will be used.

### 9.1. Car-like robot model

**Definition 9.1** The rear wheel driven vehicle with front wheel steering is a disk with radius $r_v$ and is positioned at center $(x, y)$. The vehicle is precisely described as the set

$$C = \{(z_1, z_2) \in \mathbb{R}^2 : (z_1 - x)^2 + (z_2 - y)^2 \le r_v^2\}. \quad (40)$$

The rear wheel driven vehicle with front wheel steering is shown in Fig. 7. The distance between the two axles is $\eta$ and the length of each axel is l. Thus, the kinematic model of the vehicle with respect to its center $(x, y) \in \mathbb{R}^2$ is

$$\left.\begin{aligned}\dot{x} &= v\cos\theta - \frac{\eta}{2}w\sin\theta,\\ \dot{y} &= v\sin\theta + \frac{\eta}{2}w\cos\theta,\\ \dot{\theta} &= w,\end{aligned}\right\} \quad (41)$$

where the variable $\theta$ gives the vehicle's orientation with respect to the $z_1$-axis of the $z_1 - z_2$ cartesian plane, and $v$ and $w$ are the translational and rotational velocities, respectively.[35] To ensure that the vehicle steers safely pass static obstacles, the vehicle is enclosed by the smallest possible circle that is a protective circular region centered at $(x, y)$, with radius $r_v := \frac{\sqrt{(2\epsilon_1+\eta)^2+(2\epsilon_2+l)^2}}{2}$ where $\epsilon_1 > 0$ and $\epsilon_2 > 0$ are the clearance parameters. Therefore, the definition of the vehicle is taken as equation (3) and the switched system consists of the vehicle $C$.

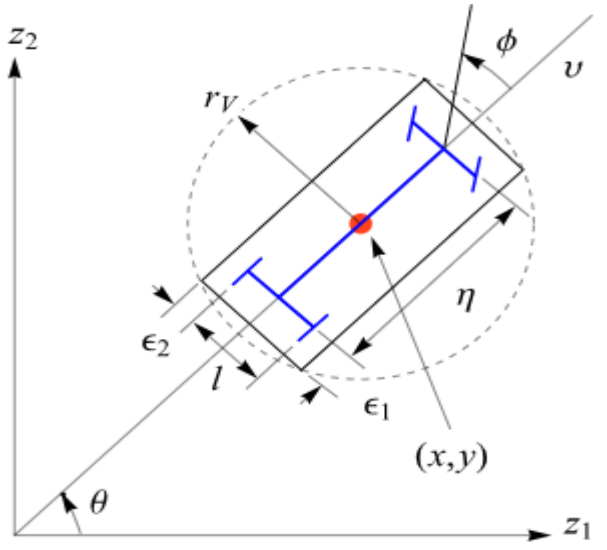


**Fig. 7** Schematic representation of the rear wheel driven car-like vehicle with front wheel steering and steering angle $\phi$.

The same multiple Lyapunov functions (9) and (25) derived for the switched system (18) and (31) will be used for the system (41) with an extension to the definition of the independent variable from $\mathbf{x} := (x, y) \in \mathbb{R}^2$ to $\boldsymbol{q} := (x, y, \theta) \in \mathbb{R}^3$ with the initial conditions vector denoted by $q_0 := (q(0)) \in \mathbb{R}^3$. Thus, the state space representation of the car like robot is

$$\dot{q} = G_p(q), q(t_0) = q_0, t \geq 0 \quad (42)$$

where $\boldsymbol{G_p}$ is a $3 \times 1$ vector with entries consisting of the righthand side terms in (41).

As stated above, the multiple Lyapunov functions for (42) is the same as (11) and (25) but with independent variable $\boldsymbol{q}$ rather than $\mathbf{x}$.

### 9.2 Scenario 1: Landmarks in hierarchical order in unconstrained environment

The system of ODEs (42) is substituted into the time derivative of (9) as shown below:

$$\dot{L}_{1_p}(\boldsymbol{q}) = f_{1_p}(\mathbf{x})\dot{x} + g_{1_p}(\mathbf{x})\dot{y}$$
$$= f_{1_p}(\mathbf{x})\left(v\cos\theta - \frac{\eta}{2}w\sin\theta\right) + g_{1_p}(\mathbf{x})\left(v\sin\theta + \frac{\eta}{2}w\cos\theta\right)$$
$$= \left(f_{1_p}(\mathbf{x})\cos\theta + g_{1_p}(\mathbf{x})\sin\theta\right)v - \frac{\eta}{2}\left(f_{1_p}(\mathbf{x})\sin\theta - g_{1_p}(\mathbf{x})\cos\theta\right)$$

#### 9.2.1 Steering control laws

The steering control laws could be accordingly defined as

$$\left.\begin{aligned} v &:= -\kappa\left(f_{1_p}(\mathbf{x})\cos\theta + g_{1_p}(\mathbf{x})\sin\theta\right),\\ w &:= \frac{2\kappa}{\eta}\left(f_{1_p}(\mathbf{x})\sin\theta - g_{1_p}(\mathbf{x})\cos\theta\right),\end{aligned}\right\} \quad (43)$$

where $\kappa$ is some arbitrary continuous positive function of $x$ and $y$ and $f_{1_p}(\boldsymbol{x})$ and $g_{1_p}(\boldsymbol{x})$ are defined in (14) and (15). With respect to system (41) and with the control laws mentioned above, the following is obtained:

$$\dot{L}_{1_p}(\boldsymbol{q}) = -\frac{1}{\kappa}\left(v^2 + \frac{\eta^2}{4}w^2\right) \leq 0.$$

Thus, system (41) can be expressed as

$$\left.\begin{aligned}\dot{x} &= -\kappa f_{1_p}(\mathbf{x}),\\ \dot{y} &= -\kappa g_{1_p}(\mathbf{x}),\\ \dot{\theta} &= \frac{2\kappa}{\eta}\left(f_{1_p}(\mathbf{x})\sin\theta - g_{1_p}(\mathbf{x})\cos\theta_i\right).\end{aligned}\right\} \quad (44)$$

The position of the vehicle $\left(x(t), y(t)\right)$ are governed by first two terms of (44) while the third governs its orientation.

#### 9.2.2 Maximum velocity

Practically, there are restrictions on the velocity and steering angle of a vehicle. A vital role is performed by the function $\kappa = \kappa(x, y) > 0$ in restricting the sizes of $v$, $w$ and the steering angles $\phi$.

Given any real number $\chi > 0$, then, from (43),

$$\left.\begin{aligned}|v| &\leq \kappa\left(\chi + \left|f_{1_p}(\mathbf{x})\right| + \left|g_{1_p}(\mathbf{x})\right|\right),\\ |w| &\leq \frac{2\kappa}{\eta}\left(\chi + \left|f_{1_p}(\mathbf{x})\right| + \left|g_{1_p}(\mathbf{x})\right|\right),\end{aligned}\right\} \quad (45)$$

If $v_{max} := |v|$ is the maximum translational speed, then from the first inequality of (45)

$$\kappa := \frac{v_{max}}{\chi + \left|f_{1_p}(\mathbf{x})\right| + \left|g_{1_p}(\mathbf{x})\right|} \quad (46)$$

#### 9.2.3 Maximum steering angle

Moveover, the size of steering angle $\phi$ is restricted using (45) and (46). Let the maximum steering angle be $\phi_{max} := |\phi|$, where $0 < \phi_{max} < \frac{\pi}{2}$. Then

$$|v| \leq v_{max} \quad and \quad v^2 \geq \rho^2 w^2 \quad where \quad \rho := \frac{\eta}{tan\phi_{max}} \quad (47)$$

are the constraints imposed on the translational velocity, $v$, and the rotational velocity $w$ as shown in Ref. [36].

From (47), there is

$$|w| \leq \left|\frac{v}{\rho}\right| \leq \frac{v_{max}}{|\rho|} \quad (48)$$

Moreover, from (45), (46) and (48), the following is obtained:

$$|w| \leq \frac{2\kappa}{\eta}\left(\chi + \left|f_{1_p}(\mathbf{x})\right| + \left|g_{1_p}(\mathbf{x})\right|\right) \quad and \quad |w| \leq \frac{v_{max}}{|\rho|}\left(\chi + \left|f_{1_p}(\mathbf{x})\right| + \left|g_{1_p}(\mathbf{x})\right|\right).$$

Let $|\rho| = \frac{\eta}{2}$ and from (47), there is $tan\phi_{max} = 2$. Thus $\phi_{max} = tan^{-1}2$ and hence the maximum steering angle of every vehicle is set at $\phi_{max} = tan^{-1}2$.

**9.3 Scenario 2**: Landmarks in hierarchical order in constrained environment

The system of ODEs (42) is substituted into the time derivative of (25) as shown below:

$$\dot{L}_{2_p}(\boldsymbol{q}) = f_{2_p}(\mathbf{x})\dot{x} + g_{2_p}(\mathbf{x})\dot{y}$$
$$= f_{2_p}(\mathbf{x})\left(vcos\theta - \frac{\eta}{2}wsin\theta\right) + g_{2_p}(\mathbf{x})\left(vsin\theta + \frac{\eta}{2}wcos\theta\right)$$
$$= \left(f_{2_p}(\mathbf{x})cos\theta + g_{2_p}(\mathbf{x})sin\theta\right)v$$
$$-\frac{\eta}{2}\left(f_{2_p}(\mathbf{x})sin\theta - g_{2_p}(\mathbf{x})cos\theta\right)w.$$

where $f_{2_p}(\mathbf{x})$ and $g_{2_p}(\mathbf{x})$ are defined in (28) and (29).

The steering control laws and the restrictions on velocity as given in Case 1 as (43) and (46) will be used with $f_{2_p}$ and $g_{2_p}$ instead of $f_{1_p}$ and $g_{1_p}$. Similarly, the same maximum steering angle for the vehicle as set in Case 1 will be used.

### 9.3.1 Detection region of the car-like vehicle

The rear-wheel-drive vehicle with front wheel steering shown in Fig. 7 with its detection region is shown in Fig. 8. The system of ODEs (42) is substituted into the time derivative of equation (25) which is governed by equation (39). The steering control laws and the restrictions on velocity as given in Case 1 as (43) and (46) will be used with $f_{2_p}$ and $g_{2_p}$ instead of $f_{1_p}$ and $g_{1_p}$. Similarly, the same maximum steering angle for the vehicle as set in Case 1 will be used.

### 9.4. Simulation results for the car-like vehicle system

System (42) was numerically simulated using RK4 method and the following values for the car-like vehicle was used in all the simulations:

- Clearance parameters: $\epsilon_1 = \epsilon_2 = 0.2$;
- Width and length of the vehicle: $l = 2, \eta = 4$;
- Radius of circular protective region: $r_v \approx 2.51$;
- Maximum speeds and steering angle: $v_{max} = 1$ and $\phi_{max} = tan^{-1}2$;
- $\chi = 1$ in $\kappa$ defined as in (46);
- Initial Orientation ($\theta$): randomized between $-\pi$ and $\pi$.

#### 9.4.1 Landmarks in hierarchical order in an unconstrained environment

Example 9.2. In this example, a car-like vehicle has to navigate to its target location via five landmarks. Fig. 9(a) shows the trajectory of the vehicle from its initial position to its target location via five landmarks. As illustrated in Fig. 9(a), the vehicle moves from its initial position via the landmarks provided in hierarchical order before finally converging at the target. The velocity graph in Fig. 9(c) shows a rapid deceleration as the vehicle approaches its final target. As time involves, the orientation angle of the vehicle changes as shown in Fig. 9(c). For this arrangement, $\gamma = 0.5$, and $\alpha_p = 1$.

#### 9.4.2 Landmarks in hierarchical order in a constrained environment

**Example 9.3.** In this example, a vehicle has to navigate to its target location via three landmarks, and in the presence of the six static obstacles. Fig. 10(a) shows the vehicle's trajectory

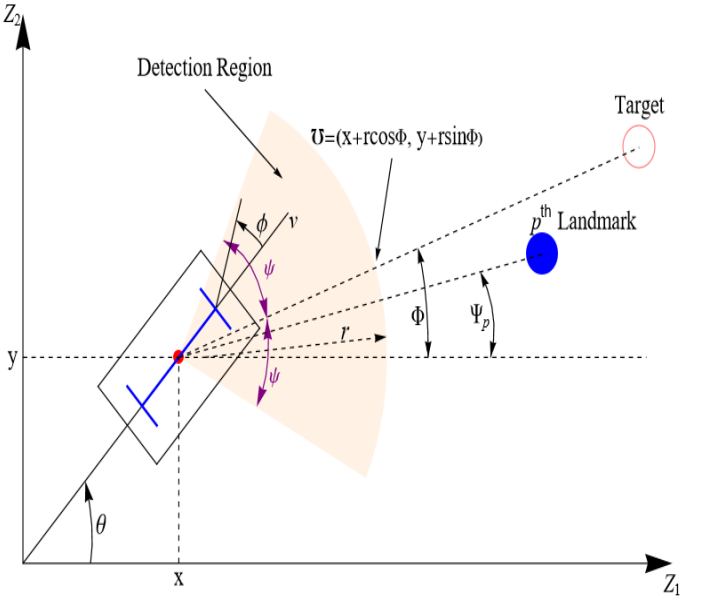


**Fig. 8** Car-like vehicle with a detection region.

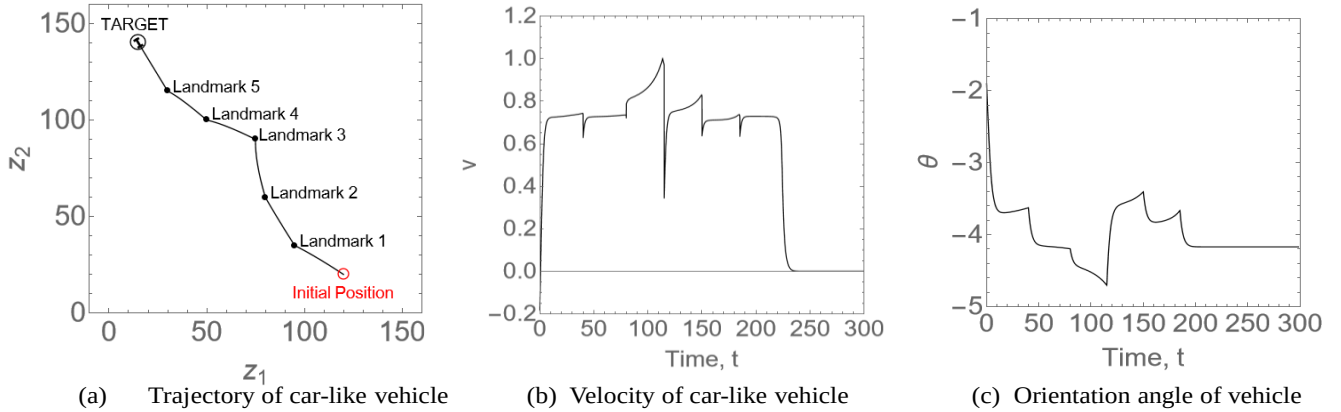


(a) Trajectory of car-like vehicle (b) Velocity of car-like vehicle (c) Orientation angle of vehicle

**Fig. 9** (a) Trajectory of the vehicle and where it ceased motion. (b) The instantaneous velocity showing rapid deceleration of the vehicle as it approaches the landmarks and the target. (c) The change of the angular orientation of the vehicle over time.

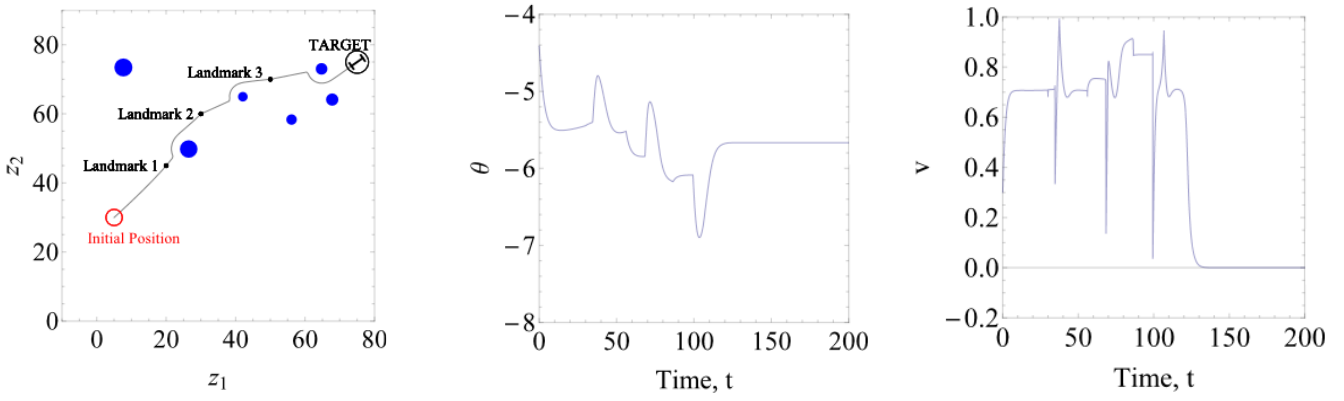


(a) Trajectory of car-like vehicle (b) Velocity of car-like vehicle (c) Orientation angle of vehicle

**Fig. 10** (a) Initial position of the vehicle and randomly generated obstacles with the position where the vehicle ceased motion. (b) The instantaneous velocity showing rapid deceleration of the car-like vehicle as it approaches the landmarks and the target. (c) The change of the angular orientation of the car-like vehicle over time as it approaches each landmark along its trajectory.

and final orientation. The vehicle moves from its initial position via the three landmarks in hierarchical order before finally converging at the target in an obstacle-ridden environment, as illustrated in Fig 10(a). The evolution of the velocity along the vehicle's trajectory is shown in Fig. 10(b). The angular orientation of the vehicle changes over time, abiding system restrictions and limitations, and is shown in Fig. 10(c) For this arrangement, $\gamma = 0.5$, $\alpha_p = 1$, and $\beta_k = 0.0001$.

### 9.4.3 Car-like vehicle with a detection region for landmarks in a constrained environment

**Example 9.4.** In this example, the position of the car-like vehicle with its detection region at time different time $t$ during its motion has been captured and illustrated in Fig. 11. The initial and final positions of the car-like vehicle are $(3,2)$ and $(25,25)$, respectively. The positions of the $n = 30$ landmarks and $q = 15$ obstacles are randomly generated with $r = 5$ and $\psi = \frac{\pi}{4}$ as the range of the detection region. For this arrangement, $\mu = \varphi = 1$, $\lambda = 0.05$, $\gamma = 0.05$ and $\beta_k = 0.001$.

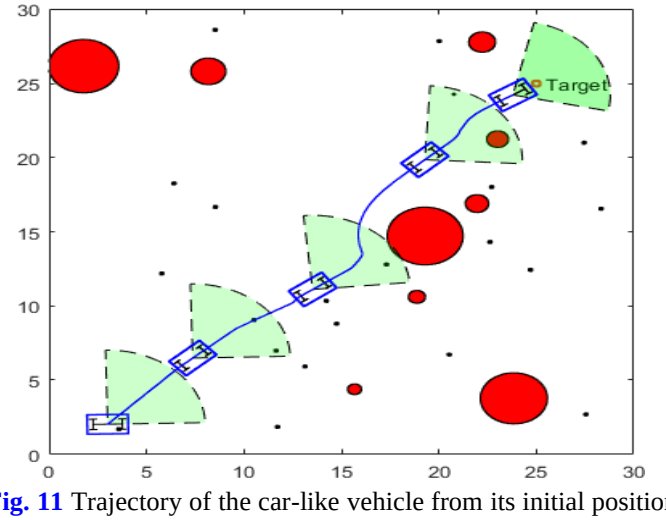


**Fig. 11** Trajectory of the car-like vehicle from its initial position to its target via extracting landmarks.

## 10. Discussion

This paper addresses motion planning in autonomous mobile robot navigation. The proposed nonlinear stabilizing switched control laws ensure continuous collision-free paths that connect an initial configuration to a goal configuration via multiple artificial hierarchal landmarks (way-points) in a possibly cluttered environment. Moreover, a landmark extracting technique has also been proposed, which enables a robot to identify action landmarks. The switched controls were successful in the motion control of a planar point-mass object and a nonholonomic car-like vehicle governed by its kinematic equations.

The simulation results of Example 6.1, Example 7.2, Example 8.2, Example 9.2, Example 9.3 and Example 9.4 show the effectiveness of the control laws. The simulation results indicate that the proposed control laws are feasible, effective, and facilitate a safe, shortest route and continuous path. It is observed that under the proposed switched controllers, the planar point-mass object and the nonholonomic car-like vehicle successfully reached its target in all the scenarios. To add on, the behavior of the multiple Lyapunov functions indicate that the planar point-mass object had no difficulty in converging to its targets.

After implementing to a point-mass object, the landmark extraction methodology and controllers designed in this research were successfully applied to a real-life mechanical system modeled as a car-like robot. The proposed landmark extraction technique ensures that all other landmarks are automatically discarded apart from the selected action landmarks. Moreover, the continuous multiple Lyapunov functions and the velocity-based controllers guarantee smooth trajectories at all points, including the hierarchal landmarks. A significant advantage of the hierarchal landmark-based navigation presented in this research is that the technique has been applied to mobile robots, which have greater mobility in a cluttered environment. In comparison, the hierarchal landmark-based navigation utilized in Refs. [22] and [23] was

 

implemented on anchored manipulators that operated from a fixed position and had limited access in the workspace. Furthermore, the proposed landmark extraction technique addresses the problem of detecting and selecting action landmarks amongst the presence of multiple landmarks in a cluttered environment. Therefore, for hierarchal landmark-based navigation, the proposed method is a better option than the approaches presented in Refs. [24] and [25], which failed to address the vital process of landmark detection and selection, especially in an environment cluttered with multiple landmarks and obstacles.

The switched control laws presented in this research is applicable to the industrial sector such as aerospace and aviation, automotive, engineering, construction and building. Specifically, when the workspace is constrained, goods or workers have to be transported from one station to other stations. Then, the proposed control laws could be used to automate the process. The major drawback of LbCS is the introduction of local minima.

### Limitations

The limitations of this study are:

- The presence of algorithm singularities in the form of local minima as LbCS is based on the classical method of the artificial potential field approach. In this study, such cases where the point-mass object and the nonholonomic car-like robot could get trapped in local minima were avoided through the selection of specific initial conditions and assigning specific values to the control, convergence and avoidance parameters using brute force technique.
- The authors have restricted themselves to using numerical proofs and computer-based simulations of interesting scenarios to demonstrate the effectiveness of the velocity-based control laws. This paper provides a theoretical exposition of the LbCS's applicability only and the velocity control laws achieved were not integrated onto some prototype experimental robot for practical results.
- The control, convergence and avoidance parameters used have not been optimized.
- The control laws achieved cannot address a dynamic environment.

## 11. Conclusion

Landmark-based navigation is an essential component of robotic systems that enhances their navigation accuracy, reliability, and efficiency. As such, it is a highly active area of research with ongoing efforts to improve and optimize landmark detection, feature extraction, and path planning algorithms. This paper presented the navigation of a point-mass object to its target via multiple hierarchal landmarks. The translational velocities of the point-mass object were constructed using a switched system of multiple Lyapunov-like functions in unconstrained and constrained environments. A new methodology was also provided to extract action landmarks from multiple landmarks in the workspace of a point-mass object. The method was applied successfully to a planar nonholonomic car-like vehicle governed by its kinematic equations. The simulation results and the behaviour of the multiple Lyapunov functions demonstrate that the planar point-mass object and the nonholonomic car-like vehicle had no difficulty in converging to their assigned targets. Despite its limitations, the proposed approach was effective in generating collision-free paths through cluttered environments.

Future work will include developing a hybrid methodology combining LbCS with a heuristic method, flushing off the drawbacks of LbCS, for landmark-based navigation and experimentally verifying the results by integrating the control laws on a prototype robot. The potential applications of this research include automating the transportation of goods or workers between different stations. Overall, the proposed approach offers a promising solution to enhance the navigation accuracy of robotic applications for more complex systems.

### Conflict of Interest

There is no conflict of interest.

### Supporting Information

Not applicable.

### References

[1] H. G. Tanner, S. G. Loizou, K. J. Kyriakopoulos, Nonholonomic navigation and control of cooperating mobile manipulators, *IEEE Transactions on Robotics and Automation*, 2003, **19**, 53-64, doi: 10.1109/TRA.2002.807549.

[2] L. J. Pinto, D.-H. Kim, J. Y. Lee, C.-S. Han, Development of a Segway robot for an intelligent transport system. 2012 IEEE/SICE International Symposium on System Integration (SII). December 16-18, 2012, Fukuoka, Japan. IEEE, 2013, 710-715, doi: 10.1109/SII.2012.6427308.

[3] J. Raj, K. Raghuwaiya, R. Havea, J. Vanualailai, Autonomous control of multiple quadrotors for collision-free navigation, *IET Control Theory & Applications*, 2023, **17**, 868-895, doi: 10.1049/cth2.12420.

[4] D. Kim, D. Lee, H. Myung, H.-T. Choi, Artificial landmark-based underwater localization for AUVs using weighted template matching, *Intelligent Service Robotics*, 2014, **7**, 175-184, doi: 10.1007/s11370-014-0153-y.

[5] S. G. Tzafestas, Mobile manipulator modeling and control. Introduction to Mobile Robot Control. Amsterdam: Elsevier, 2014: 385-428, doi: 10.1016/b978-0-12-417049-0.00010-9.

[6] J. Raj, K. S. Raghuwaiya, J. Vanualailai, Novel Lyapunov-based autonomous controllers for quadrotors, *IEEE Access*, 2020, **8**, 47393-47406, doi: 10.1109/ACCESS.2020.2979223.

[7] C. D. Makavita, H. D. Nguyen, D. Ranmuthugala, S. G. Jayasinghe, Composite model reference adaptive control for an unmanned underwater vehicle, *Underwater Technology*, 2015, **33**, 81-93, doi: 10.3723/ut.33.081.

[8] A. J. Briggs, C. Detweiler, D. Scharstein, A. Vandenberg-

Rodes, Expected shortest paths for landmark-based robot navigation, *The International Journal of Robotics Research*, 2004, **23**, 717-728, doi: 10.1177/0278364904045467.
[9] X. Wang, S. X. Yang, A neuro-fuzzy approach to obstacle avoidance of a nonholonomic mobile robot. Proceedings 2003 IEEE/ASME International Conference on Advanced Intelligent Mechatronics (AIM 2003), Kobe, Japan, 2003, **1**, 29-34, doi: 10.1109/AIM.2003.1225067.
[10] E. Keyder, S. Richter, M. Helmert, Sound and complete landmarks for and/or graphs, in: H. Coelho, R. Studer, M. Wooldridge (Eds.), ECAI 2010, 19th European Conference on Artificial Intelligence, IOS Press, 2010, 335–340, doi: 10.3233/978-1-60750-606-5-335.
[11] M. Elkawkagy, B. Schattenberg, S. Biundo-Stephan, Landmarks in hierarchical planning, in: H. Coelho, R. Studer, M. Wooldridge (Eds.), ECAI 2010, 19th European Conference on Artificial Intelligence, IOS Press, 2010, 229–234. doi:10.3233/978-1-60750-606-5-229.
[12] D. Busquets, C. Sierra, R. L. De Mantaras, A multiagent approach to qualitative landmark- based navigation, *Autonomous Robots*, 2003, **15**, 129–154, doi: 10.1023/A:1025536924463.
[13] A. Lazanas, J.-C. Latombe, Landmark-based robot navigation, *Algorithmica*, 1995, **13**, 472-501, doi: 10.1007/BF01190850.
[14] C. Owen, U. Nahmzow, Landmark-Based Navigation for a Mobile Robot, in: From Animals to Animats 5: Proceedings of the Fifth International Conference on Simulation of Adaptive Behavior, The MIT Press, 1998, doi: 10.7551/mitpress/3119.003.0037.
[15] A. Bais, R. Sablatnig, J. Gu, Single landmark based self-localization of mobile robots. The 3rd Canadian Conference on Computer and Robot Vision (CRV'06). June 7-9, 2006, Quebec, Canada. IEEE, 2006, 67, doi: 10.1109/CRV.2006.67.
[16] I. Shimshoni, On mobile robot localization from landmark bearings, *IEEE Transactions on Robotics and Automation*, 2002, **18**, 971-976, doi: 10.1109/TRA.2002.805663.
[17] H. Fujii, Y. Ando, T. Yoshimi, M. Mizukawa, Shape recognition of metallic landmark and its application to self-position estimation for mobile robot, *Journal of Robotics and Mechatronics*, 2010, **22**, 718-725, doi: 10.20965/jrm.2010.p0718.
[18] H. Hu, D. Gu, Landmark-based navigation of mobile robots in manufacturing. 1999 7th IEEE International Conference on Emerging Technologies and Factory Automation. Proceedings ETFA '99 (Cat. No.99TH8467). October 18-21, 1999, Barcelona, Spain. IEEE, 2002, 121-128, doi: 10.1109/ETFA.1999.815346.
[19] R. Lerner, E. Rivlin, I. Shimshoni, Landmark selection for task-oriented navigation. 2006 IEEE/RSJ International Conference on Intelligent Robots and Systems. October 9-15, 2006, Beijing, China, IEEE, 2007, 2785-2791, doi: 10.1109/IROS.2006.282060.
[20] O, Wijk, Localization and navigation of a mobile robot using natural point landmarks extracted from sonar data, *Robotics and Autonomous Systems*, 2000, **31**, 31-42, doi: 10.1016/S0921-8890(99)00085-8.
[21] B. Sharma, A. Prasad, R. Chand, S. Kumar, J. Raj, J. Vanualailai, Landmarks as navigation-aids for multiple robots. 2020 Fourth International Conference on Inventive Systems and Control (ICISC). January 8-10, 2020, Coimbatore, India. IEEE, 2020, 8-14, doi: 10.1109/ICISC47916.2020.9171123.
[22] R. Chand, S. A. Kumar, R. P. Chand, Navigation of an n-link revolute robotic arm via hierarchal landmarks. 2021 3rd Novel Intelligent and Leading Emerging Sciences Conference (NILES). October 23-25, 2021, Giza, Egypt, IEEE, 2021, 188-192, doi: 10.1109/NILES53778.2021.9600539.
[23] R. Chand, R. P. Chand, S. A. Kumar, Switch controllers of an *n*-link revolute manipulator with a prismatic end-effector for landmark navigation, *PeerJ Computer Science*, 2022, **8**, e885, doi: 10.7717/peerj-cs.885.
[24] A. Prasad, B. Sharma, S. A. Kumar, Strategic creation and placement of landmarks for robot navigation in a partially-known environment. 2020 IEEE Asia-Pacific Conference on Computer Science and Data Engineering (CSDE). December 16-18, 2020, Gold Coast, Australia. IEEE, 2021, 1-6, doi: 10.1109/CSDE50874.2020.9411583.
[25] S. A. Kumar, B. Sharma, J. Vanualailai, A. Prasad, Stable switched controllers for a swarm of UGVs for hierarchal landmark navigation, *Swarm and Evolutionary Computation*, 2021, **65**, 100926, doi: 10.1016/j.swevo.2021.100926.
[26] D. Liberzon, A. S. Morse, Basic problems in stability and design of switched systems, *IEEE Control Systems Magazine*, 1999, **19**, 59-70, doi: 10.1109/37.793443.
[27] M. S. Branicky, Multiple Lyapunov functions and other analysis tools for switched and hybrid systems, *IEEE Transactions on Automatic Control*, 1998, **43**, 475-482, doi: 10.1109/9.664150.
[28] M. Torres-Torriti, P. Nazate-Burgos, F. Paredes-Lizama, J. Guevara, F. Auat Cheein, Passive landmark geometry optimization and evaluation for reliable autonomous navigation in mining tunnels using 2D lidars, *Sensors*, 2022, **22**, 3038, doi: 10.3390/s22083038.
[29] M. Tedder, P. Cao, B. P. Grote, E. L. Hall, Global-local navigation using a GPS, Intelligent Engineering Systems through Artificial Neural Networks, ANNIE 13.
[30] R. Vázquez-Martín, P. Núñez, A. Bandera, F. Sandoval, Curvature-based environment description for robot navigation using laser range sensors, *Sensors*, 2009, **9**, 5894-5918, doi: 10.3390/s90805894.
[31] R. Bączyk, A. Kasiński, P. Skrzypczyński, Vision-based mobile robot localization with simple artificial landmarks, *IFAC Proceedings Volumes*, 2003, **36**, 201-206, doi: 10.1016/s1474-6670(17)33393-1.
[32] M. Beinhofer, J. Müller, A. Krause, W. Burgard, Robust landmark selection for mobile robot navigation. 2013 IEEE/RSJ International Conference on Intelligent Robots and Systems. November 3-7, 2013, Tokyo, Japan. IEEE, 2014, 3637-2643, doi: 10.1109/IROS.2013.6696728.
[33] B. Sharma, J. Vanualailai, S. Singh, Tunnel passing maneuvers of prescribed formations, *International Journal of Robust and Nonlinear Control*, 2014, **24**, 876-901, doi: 10.1002/rnc.2923.

 

[34] J. Vanualailai, J.-H. Ha, S.-I. Nakagiri, A solution to the two-dimensional findpath problem, *Dynamics and Stability of Systems*, 1998, **13**, 373-401, doi: 10.1080/02681119808806270.
[35] J. Vanualailai, B. Sharma, S.-I. Nakagiri, An asymptotically stable collision-avoidance system, *International Journal of Non-Linear Mechanics*, 2008, **43**, 925-932, doi: 10.1016/j.ijnonlinmec.2008.06.012.
[36] G. J. Pappas, K. J. Kyriakopoulos, Stabilization of non-holonomic vehicles under kinematic constraints, *International Journal of Control*, 1995, **61**, 933-947, doi: 10.1080/00207179508921939.